Gravitational collapse in Einstein-Gauss-Bonnet gravity

Ayan Chatterjee[*] and Suresh C. Jaryal[†]
Department of Physics and Astronomical Science, Central University of Himachal Pradesh, Dharamshala-176206, India

Avirup Ghosh[‡]
Interdisciplinary Center for Theoretical Study, University of Science and Technology of China, Peng Huanwu Center for Fundamental Theory, Hefei, Anhui 230026, China

(Received 26 October 2021; accepted 1 August 2022; published 23 August 2022)

In this paper, we study gravitational collapse in the 5-dimensional Einstein-Gauss-Bonnet (EGB) theory. We construct the spherical marginally trapped surfaces and determine their evolution when the collapsing matter admits a wide class of initial density distributions. We show that their location, and time of formation depend crucially on the initial density, and the initial velocity profile of collapsing matter, as well as on the Gauss-Bonnet (GB) coupling constant. In particular, trapped surfaces only appear when the mass contained inside the collapsing spherical shell is greater or equal to the GB coupling. Otherwise, no trapped surfaces exist and the central singularity is massive and naked. This inference is verified for pressureless dust and extended for fluids satisfying equations of state. We also make a detailed comparison of these results with those in Einstein's theory; the effect of dimensionality of spacetime on these results is discussed as well.

DOI: 10.1103/PhysRevD.106.044049

I. INTRODUCTION

The study of gravitational collapse of a self-gravitating isolated system remains a matter of great physical importance in understanding large scale structures in the universe, as well as toward discerning the formation of black hole horizons, spacetime singularities and the cosmic censorship conjecture [1–6]. In general relativity (GR), the spherical gravitational collapse and the singularity theorems have been studied at length. Although several important aspects including the cosmic censorship, nonsymmetrical collapse remain to be understood completely, progress in this direction has been remarkable.

The models of gravitational collapse in alternate theories of gravity, including higher dimensional ones are also being studied with interest since it is believed that one (or some) of these theories may solve problems affecting GR, including spacetime singularities [7–14]. Among these, modified gravity theories with higher curvature corrections arise naturally. Indeed, GR is viewed as an effective field theory in which the Einstein-Hilbert action is only a low energy contribution and higher curvature terms consistent with diffeomorphism invariance may become relevant as one goes to higher energies [15–22]. Such higher curvature terms have been explicitly obtained in string theories [23–27]. These higher curvature corrections should leave imprints at low energy scales which become important for low energy physics too, affecting the horizon structure of large black holes. The Einstein-Gauss-Bonnet (EGB) theory is the simplest diffeomorphism invariant modification of GR whose equations of motion contain no more than second order in time derivatives [16–18,28–30]. This generalization is also known to be the unique lowest order correction in the Lovelock action. Furthermore, since the EGB gravity is free from ghosts (if the coupling constant has the same sign as the GR term) and leads to a well-defined initial value problem, it is a respectable theory of gravity in higher dimensions, and its solutions have also been a matter of interest. In particular, black hole solutions in the EGB theory are well known. They include the Boulware-Deser, and other spherically symmetric solutions [25,31–33]. Black holes in EGB theory are also testing grounds to gain fundamental insights into various quantum aspects of gravity like the horizon entropy [34–36].

Thus, because of the importance of the EGB theory as a natural higher dimensional theory, effects of the GB correction term on singularity formation have received attention. In the literature, inhomogeneous dust collapse of Lemaitre-Tolman-Bondi (LTB) type, and of null dust have been discussed [7–12]. These studies indicate that the central (as well as noncentral) singularity is naked, and this untrapped region increases with coupling constant $\lambda > 0$. However, it remains a possibility that such singularities may not exist if realistic matter density distributions are

[*]ayan.theory@gmail.com
[†]suresh.fifthd@gmail.com
[‡]avirup@ustc.edu.cn

considered. This expectation is not unwarranted since occurrence of these singularities break the censorship conjecture [6], as well as the Seifert conjecture [37], which essentially states that massive singularities must be censored inside a trapped region. Of course, it remains a possibility that these conjectures themselves need modifications in higher dimensions, just like the Hoop conjecture [38]. Hence, it is essential that gravitational collapse in the EGB model be studied in a greater generality, using a large class of models where the matter admits a wide variety of initial density and velocity profiles so that gravitational collapse may be understood in significant detail. To obtain this broader picture of the collapse process, we need to understand the formation of spacetime singularity, and simultaneously track the horizon formation as the shells of matter collapse. A delay in the time of formation, of one over the other, leads either to a naked singularity or to a black hole. In other words, to unambiguously certify the outcome of a specific collapse process in EGB theory, exact radius–time relation of shells is necessary.

However, studies carried out so far have been focused on obtaining the nature of singularity using behavior of geodesics near the center of the matter distribution [7–9]. The density distribution of matter is taken to be of simple power- law type. Although such techniques lead to a qualitative understanding of the process, exact solutions are better. The only explicit solution of shell collapse have been for marginally bound inhomogeneous dust models admitting power law density profile [11]. For a more complete picture, individual shell dynamics is a necessary requirement, and such studies must be carried out for matter possessing diverse energy- momentum tensors. This analysis is yet to be carried out. So, to address this lacunae in the literature, we formulate the problem of gravitational collapse in 5d EGB by directly solving the field equations of matter shells. Why 5d EGB theory? As we shall see, in this dimension, interesting features like massive naked singularities, and horizons both arise, depending on matter and geometric parameters, So, it forms an ideal testing ground for scrutinising our perceptions. These studies shall then be extended to dimensions $n > 5$, to identify the region of the parameter space where singular structures arise.

In the following, we shall explicitly solve the 5d EGB field equations describing gravitational collapse of inhomogeneous dust and of fluids satisfying equations of state. By assuming that the initial matter profile is either (a) marginally bounded, (b) bounded,[1] we shall be able to determine the radius of collapsing shell as a function of shell coordinate and its proper time. These solutions shall be used to obtain the singularity formation time. We shall also locate the time of formation of spherically symmetric trapped surfaces, and determine the evolution of their boundary (considered as the black hole horizon here) as matter falls in. Note that the formation of spacetime singularity, trapped surfaces, and their time development depend not only on the theory, or the initial velocity profile, but is also intimately connected with the density distribution of the collapsing matter. For example in GR, the formation and dynamics of the black hole horizon changes drastically with variations in the density profile [39,40], and it is natural to expect that such various shall be observed for the GB modification too. To include these variation, we study the above-mentioned objectives using spherical shells of inhomogeneous pressureless matter admitting a wide range of realistic initial density distribution profile. In each of the examples, we shall track the motion of individual collapsing matter shells, simultaneously follow the time development of spacetime singularity, and determine the trapped region formed due to these shells. We shall also be able to precisely quantify location and time of occurrence of the black hole horizon, and detail its development as more matter falls through it. This will allow us to identify the singularity is censored or covered by the horizon. In particular, we shall show that (i) for $n = 5$, unless mass $\geq 2\lambda$ no trapped surface exists (ii) trapped surfaces always exist for spacetimes in $n \geq 6$, admitting arbitrary mass. A consequence of these conclusions are that black hole horizons censor a singularity in $n = 5$, only when sufficient mass $\geq 2\lambda$ has collapsed, and that singularities in $n \geq 6$ are always censored.

Note that in gravitational collapse, the fundamental role is played by trapped surfaces. The boundary of these trapped surfaces is also defined as a black hole horizon. We present a brief motivation for this alternate approach: Black hole horizons are usually defined through event horizons [1,2]. This definition suffers from theoretical inconsistencies due to its teleological nature and hence, there has been a surge of interest toward a quasilocal definition of horizons [41]. In the following, we exploit this quasilocal method and consider the horizon to be a 4-dimensional null hypersurface foliated by closed spherical 3-dimensional spacelike spheres, such that the expansion scalar of the outgoing null normal to the foliation (ℓ^μ) vanishes, $\theta_{(\ell)} = 0$, while the expansion of the ingoing null normal to the foliation, (n^μ) is negative $\theta_{(n)} < 0$. This formulation of the black hole horizon is called marginally trapped tube (MTT) and has found use in analytical and numerical studies of black holes. In particular, MTT has helped in understanding their classical nature, quantum behavior, as well as their stability under various geometric and physical variations [39,41–58]. Note that although MTT is not associated with a particular signature, it can describe various states of a horizon. For example, a black hole horizon in equilibrium is a null MTT and is referred to as an isolated horizon (IH) (see [41,43,44,53,58]. Here, the tangent vector field of the MTT is null. A growing black hole admits a spacelike tangential vector

[1]An extension for unbounded collapse is similar and shall not been carried out here.

field, and this MTT is called a dynamical horizon (DH) (see [41,45,46,55,56] for these horizons as well as their variations). Further, it is useful to describe a MTT with timelike signature, which admits matter flow in both directions, and is called a timelike tube. Thus MTTs provide an unified framework to study time evolution of black holes through different phases. The nature of spherical MTTs during gravitational collapse in GR has been studied in detail for various class of matter fields [39,40]. However, spherical MTTs in the EGB theory remains to be studied in the context of gravitational collapse of inhomogeneous matter fields (the LTB models), and here we fill this gap by making a detail study of these matter collapse models. We carry out, (i) study the collapse end state with special emphasis on the formation of horizons, and in particular, track the location of spherical marginally trapped tubes with variation of matter profile, and (ii) for the mass profiles considered here, identify the regions of the parameter space where the MTT evolves as a DH (spacelike), where it might be timelike, and when it reaches equilibrium and become a null IH. This shall also help us to (iii) correctly locate the spherical outermost trapped surface developing during gravitational collapse. We must stress that although MTTs in 4-dimensions have been studied [39,40], their behavior is drastically different in the EGB models, even for *small* coupling constants.

The paper is arranged as follows: In the next section, we briefly discuss geometry of the MTTs, the equations of motions for the EGB theory and it's reduction in the context of spherically symmetric spacetimes using the $(t, r, \theta, \phi, \psi)$ coordinates. We shall also discuss the matter contributions to these equations and the way to determine the spherically symmetric MTTs for these spacetimes. In Sec. III, we solve the equations of motion directly for the marginally bounded and bounded cases. The solution for the unbounded case is similar, and so we shall not repeat it here. We conclude in Sec. IV with discussions. The units $c = 1$, $8\pi G = 1$ are used throughout the paper.

II. MARGINALLY TRAPPED TUBES IN THE EGB THEORY

The formalism of MTT as a quasilocal description of black hole horizons was developed in [47]. In the following, we present a brief discussion on this formalism, and set up the basic notations for our later use. Let us consider a 5-dimensional spacetime $(\mathcal{M}, g_{\mu\nu})$ with signature $(-,+,+,+,+)$. Let Δ be a hypersurface in $\mathcal{M}$ which may be spacelike, timelike or even null. Δ is taken to be topologically $S^3 \times \mathbb{R}$. At each point of the spacetime, we shall have 2 null vectors and three spacelike vectors. The null vector fields ℓ^μ and n^μ are respectively the outgoing and the ingoing vector fields orthogonal to the 3-sphere cross sections of Δ, with $\ell \cdot n = -1$. The three normalized spacelike vectors tangential to the 3- sphere are called $\hat{\theta}$, $\hat{\phi}$, and $\hat{\psi}$ respectively, and are orthogonal to the null vectors ℓ^μ and n^μ. If t^μ is a vector field tangential to Δ and normal to the S^3 foliations, then $t^\mu = \ell^\mu - Cn^\nu$, where C is a function of the foliation coordinates. Now, assume that the S^3 foliations are such that its null normals satisfy the following conditions: (i) $\theta_{(\ell)} = 0$, and (ii) $\theta_{(n)} < 0$. The hypersurface Δ foliated by such surfaces is called a MTT. Naturally MTT depends on the foliation but, in this paper, we shall restrict only to MTTs which are geometrical spheres. This means that the shear and rotation corresponding to the null normal ℓ^μ vanish on the MTT [41]. Note also that MTT does not carry a specific signature. Since $t \cdot t = 2C$, this parameter C determines the signature of Δ. When $C = 0$, Δ is null, foliated by ℓ^μ and it describes a black hole in equilibrium, a DH when it is spacelike ($C > 0$), or simply a timelike membrane when $C < 0$ and Δ is timelike. Thus, MTT is an unified formalism for horizon evolution. The value of C can be determined for various gravitational collapse processes, and for a wide class of energy momentum tensors. Hence, the entire evolution of the MTT can be unambiguously determined throughout the evolution process, if the signature of C is known.

As t^μ is orthogonal to the foliations and tangential to Δ, it generates a foliation preserving flow so that on the MTT (Δ), the following condition holds:

$$\pounds_t \theta_{(\ell)} = 0. \tag{1}$$

This equation implies that on the MTT, variation of the expansion scalar $\theta_{(\ell)}$ along null normals are related:

$$\pounds_\ell \theta_{(\ell)} = C \pounds_n \theta_\ell. \tag{2}$$

In terms of the parameter C, this is rewritten as $C = [\pounds_\ell \theta_{(\ell)} / \pounds_n \theta_{(\ell)}]$. To determine the value of C, we use the geometrical equations (B18) and (B19) of 3-surface geometry given in the Appendix B. These equations imply that on Δ, the quantity C, which determines the nature of MTT is given by:

$$C = \frac{G_{\mu\nu}\ell^\mu \ell^\nu}{3(2\pi^2/\mathcal{A})^{2/3} - G_{\mu\nu}\ell^\mu n^\nu}, \tag{3}$$

where we have used the relation between area of the round 3-sphere $\mathcal{A}$, and the scalar curvature: $\mathcal{R} = 6(2\pi^2/\mathcal{A})^{2/3}$. We shall also assume that the Einstein-Gauss-Bonnet field equations $G_{\mu\nu} \equiv R_{\mu\nu} - (1/2)Rg_{\mu\nu} = T_{\mu\nu}$,[2] holds on Δ.

[2]We use the units of $c = 1$ and $8\pi G = 1$, or equivalently, we scale the components of the energy-momentum tensor by $8\pi G$. In case of the EGB theory too, we shall write the Einstein equations in the similar manner, $G_{\mu\nu} = T_{\mu\nu}$. In that case, $T_{\mu\nu}$ shall imply a sum of terms, due to matter variables $T_{\mu\nu}$ and, due to extra geometric variables arising out of the GB correction.

The signature of C in Eq. (3) is a quantity of utmost importance since it decides the nature and *stability* of horizon [48,52], and, as may be observed from the above equation, this value is regulated by the null components of the energy- momentum tensor as well as area of the cross sections of the MTT. However, in the following sections where we shall treat a wide class of energy-momentum tensors for collapse models of the LTB type, we shall observe that details like the initial velocity profile, initial density profile of the collapsing matter, and the dimension of the spacetime play important role as well. Indeed, in several cases, simple changes in the density profile alters the nature and time of formation of the spacetime singularity, and that of the MTT quite drastically. For example, in 4-dimensions, if the matter profile is smooth, the MTT begins as a spacelike hypersurface from the center of the cloud as soon as matter begins to fall, and asymptotes to the null event horizons as infall of matter is discontinued. Trapped surfaces in 4-dimensions are discussed in [39,50,59–69]. However, in the 5-dimensional EGB theory, even for the collapse of marginally bound matter with density admitting a Gaussian distribution, the central singularity forms earlier than the corresponding MTT. This happens because the EGB equations allow the formation of MTT only at the later shell coordinates, and hence, the collapse of the first few shells leads to an untrapped singularity.

In the following section, we shall discuss the EGB equations of motion for the spherical collapse of matter fields, and determine the requirements for formation of trapped surfaces in the 5-dimensions.

A. The equations of motion

The action for the 5-dimensional EGB theory is given by

$$S = \int d^5x\sqrt{-g}(R + \lambda L_{\rm GB}) + S_{\rm matter}, \tag{4}$$

where R is the Ricci scalar, g denotes determinant of the metric $g_{\mu\nu}$ and, λ is coupling constant of the Gauss-Bonnet term. The Gauss-Bonnet Lagrangian $(L_{\rm GB})$ is given by

$$L_{\rm GB} = R^2 - 4R_{\mu\nu}R^{\mu\nu} + R_{\mu\nu\sigma\delta}R^{\mu\nu\sigma\delta}. \tag{5}$$

The action Eq. (4) leads to the following field equations

$$G_{\mu\nu} \equiv R_{\mu\nu} - \frac{1}{2}Rg_{\mu\nu} = T_{\mu\nu} - \lambda H_{\mu\nu}, \tag{6}$$

where the term $G_{\mu\nu}$ is the usual Einstein tensor as in GR, $T_{\mu\nu}$ is the energy momentum tensor, and $H_{\mu\nu}$ is the contribution due to the Gauss-Bonnet term. In the above equation (6), the term $H_{\mu\nu}$ signifies the following

$$\begin{aligned} H_{\mu\nu} &= H'_{\mu\nu} - \frac{1}{2}g_{\mu\nu}L_{\rm GB} \\ &= 2[RR_{\mu\nu} - 2R_{\mu\lambda}R^{\lambda}{}_{\nu} - 2R^{\lambda\sigma}R_{\mu\lambda\nu\sigma} + R_{\mu}{}^{\lambda\sigma\delta}R_{\nu\lambda\sigma\delta}] \\ &\quad - \frac{1}{2}g_{\mu\nu}L_{\rm GB}. \end{aligned} \tag{7}$$

Note that $H_{\mu\nu}$ may be considered as an effective energy momentum tensor adding to the usual matter tensor.

Now, we consider a general spherically symmetric collapsing cloud of fluid bounded by a spherical surface. In the comoving coordinates, the line element of a 5 dimensional spherically symmetric spacetime geometry can be written as

$$\begin{aligned} ds^2 = &-e^{2\alpha(r,t)}dt^2 + e^{2\beta(r,t)}dr^2 + R(r,t)^2[d\theta^2 + \sin^2\theta d\phi^2 \\ &+ \sin^2\theta\sin^2\phi d\psi^2], \end{aligned} \tag{8}$$

where $\alpha(r,t)$, $\beta(r,t)$ and $R(r,t)$ are metric functions to be determined.[3] $R(r,t)$ is radius of the collapsing matter cloud whereas, θ, ϕ, ψ are the angular coordinates of that 3-sphere. The energy momentum tensor for the fluid is taken to be

$$T_{\mu\nu} = (p_t + \rho)u_\mu u_\nu + p_t g_{\mu\nu} + (p_r - p_t)X_\mu X_\nu \tag{9}$$

where $\rho(r,t)$ is density, whereas $p_r(r,t)$ and $p_t(r,t)$ are the radial and tangential components of pressure. The u^μ and X^μ are unit timelike and spacelike vectors satisfying $u_\mu u^\mu = -X_\mu X^\mu = -1$ In the comoving co-ordinates the four velocity and the unit spacelike vector of the fluid as $u^\mu = e^{-\alpha}(\partial_t)^\mu$ and $X^\mu = e^{-\beta}(\partial_r)^\mu$. In the above equation, we have kept the form of the energy-momentum tensor quite general so as to write the EGB field equations in some generality, which we shall use in the Appendix A, to write the on-shell values of geometric fields in terms of the matter variables. The equation of motion for this metric in the EGB theory are given by

$$\rho(r,t) = \frac{3}{2}\frac{F'(r,t)}{R^3R'}, \tag{10}$$

$$p_r(r,t) = -\frac{3}{2}\frac{\dot{F}(r,t)}{R^3\dot{R}}, \tag{11}$$

$$\dot{R}' = \dot{R}\alpha' + R'\dot{\beta}, \tag{12}$$

$$\alpha' = \frac{3R'}{R}\frac{p_t - p_r}{\rho + p_r} - \frac{p'_r}{\rho + p_r}, \tag{13}$$

$$F(r,t) = R^2(1 - G + H) + 2\lambda(1 - G + H)^2, \tag{14}$$

[3]The symbol R is used to denote both Ricci scalar and the radius of the matter configuration. We deliberately kept the same symbol since they will not appear simultaneously to cause any confusion.

where the superscripts primes ($'$) and dots ($\cdot$) represent partial derivatives with respect to r and t respectively. The quantity $R(r,t)$ is physical radius for matter configuration and $F(r,t)$ is the Misner-Sharp mass function. The first and the second equations, (10) and (11), are the G_{00} and the G_{11} equations. The third is the R_{01} equation. The fourth equation is the Bianchi identity $\nabla_\mu T^{\mu r}=0$, which for the pressureless matter implies that the metric variable $\alpha'=0$. Equation (14), is the equation for the mass function with the functions $H(r,t)$ and $G(r,t)$ defined as $H=e^{-2\alpha}\dot{R}^2$ and $G=e^{-2\beta}R'^2$.

Several points are to be noted regarding the above-mentioned equations of motion. First, the relation between the matter variables and the geometric variables in the above Eqs. (8)–(14) are modified in comparison to the 4-dimensional Einstein theory. The changes in the numerical factors are due to dimensionality of the spacetime as well as due to change in the theory itself, see for example Eq. (14), where the mass function $F(t,r)$ is modified by the EGB coupling constant.

Second, the number of independent equations are five in number. The unknown functions in this problem are the three metric variables $\alpha(t,r)$, $\beta(t,r)$, $R(t,r)$, three matter variables $p_r(r,t)$, $p_t(t,r)$, $\rho(t,r)$, and the mass-function $F(t,r)$. This combination allows two freely specifiable functions. Since the equations give dynamical evolution of the functions, it is natural to specify these functions at an initial time $t=t_i$, and allow the Einstein equations to evolve the dynamical functions. Since we shall be dealing with pressureless (dust) collapse, it is useful to point out that for dust collapse, p_r and p_t are taken to vanish at t_i, and this fixes the function $\alpha(t,r)=\alpha(t)$. We shall show below that this effectively implies $\alpha=0$, since we can rescale the time coordinate. The remaining freely specifiable functions are the density $\rho(r,t_i)$, and $\beta(r,t_i)$ which, as we shall show below, implies the specification of initial density and velocity profiles of the collapsing matter. We shall also assume that $R(r,t_i)=r$. This requirement is consistent with the regularity conditions discussed below. By choosing different values of r at the initial surface gives the time evolution of the various shells of matter.

Thirdly, few regularity conditions on the metric functions must also be enforced during the collapse process. The positivity and regularity of the density $\rho(t,r)$, and Eq. (10) imply that the mass function $F(t,r)$ must smoothly vanish at the center of the matter configuration at $r=0$. The condition $R(t,r)=0$ is the genuine spacetime singularity where the density and the curvature scalars blow up. Note that the density also blows up for $R'=0$, although this is not a genuine spacetime singularity and can be removed. This condition in fact implies shell-crossings, when shells of fixed r cross each other. The sufficient condition which guarantees no shell-crossing is $R'>0$, which ensures that shells maintain their ordering. Note that $R(r,t_i)=r$, and any other index on r leads either to shell-crossing or affects differentiability of metric functions at center of the matter configuration. An important requirement for gravitational collapse is to require $\dot{R}(r,t)<0$. Finally, we shall ensure in our study that no trapped surface is present at the initial data, by checking that the value of r at the initial surface is greater than the condition of formation of trapped surface at that coordinate.

Now, with the metric given in Eq. (8), the outgoing and the incoming null normals to the 3-sphere are given by:

$$\ell^\mu = e^{-\alpha(r,t)}(\partial_t)^\mu + e^{-\beta(t,r)}(\partial_r)^\mu \tag{15}$$

$$n^\mu = (1/2)e^{-\alpha(r,t)}(\partial_t)^\mu - (1/2)e^{-\beta(t,r)}(\partial_r)^\mu. \tag{16}$$

This leads to the following expressions for the expansion scalars:

$$\begin{aligned}\theta_{(\ell)} &= \frac{3}{R(r,t)}[\dot{R}\exp(-\alpha)+R'\exp(-\beta)] \\ &= \frac{3}{R(r,t)}[\dot{R}+\sqrt{1-k(r)}],\end{aligned} \tag{17}$$

$$\theta_{(n)} = \frac{3}{R(r,t)}[\dot{R}\exp(-\alpha)-\sqrt{1-k(r)}], \tag{18}$$

where we have used the relation $R'=e^{\beta(r,t)}\sqrt{1-k(r)}$. This relation is obtained as follows: For the case of pressureless matter, Eq. (13) gives $\alpha'=0$ which along with Eq. (12) implies:

$$G(t,r)=e^{-2\beta(r,t)}R'^2\equiv E(r)\equiv 1-k(r), \tag{19}$$

where $k(r)$, $E(r)$ are the integration functions. From the Eq. (14), the equation of motion of collapsing configuration gives the following expression for $\dot{R}(t,r)$:

$$\dot{R}(r,t)=-e^{\alpha(t,r)}\left[(1/4\lambda)\left\{\sqrt{R^4+8\lambda F(r,t)}-R^2\right\}-k(r)\right]^{1/2}, \tag{20}$$

where we have used the $-$ve sign, as required for gravitational collapse. It follows from this Eq. (20), and the equation (17) that the condition for $\theta_{(\ell)}=0$ requires:

$$R_M(r,t)=\sqrt{F(r,t)-2\lambda}, \tag{21}$$

which at the same time is also the condition for $\theta_{(n)}<0$. Thus, for the spacetimes we are studying, all the three spheres which satisfy Eq. (21) are marginally trapped spheres.

As discussed earlier following Eq. (3), the dynamics of the marginally trapped surfaces (whether they are timelike, spacelike or null), depends upon sign of the parameter C. On the MTT, it is given by

$$C=\frac{T_{\mu\nu}\ell^\mu\ell^\nu-\lambda H_{\mu\nu}\ell^\mu\ell^\nu}{3/R(r,t)^2-T_{\mu\nu}\ell^\mu n^\nu+\lambda H_{\mu\nu}\ell^\mu n^\nu}, \tag{22}$$

where Eq. (3) and Eq. (6) have been used. Now, the task is to write down all the components in $T_{\mu\nu}$ as well as in $H_{\mu\nu}$ in terms of the matter variables. The expression for $T_{\mu\nu}$ is already given in Eq. (9). The details of the calculation for $H_{\mu\nu}$ is carried out in the Appendix A. The quantity $H_{\mu\nu}\ell^\mu\ell^\nu$ in Eq. (22) is given by:

$$H_{\mu\nu}\ell^\mu\ell^\nu = 2\left[\frac{6F(\rho+p_r)}{F^2}+2p_t^2-4p_rp_t-\frac{2}{3}p_t(\rho+p_r)\right], \tag{23}$$

Similarly, the expressions for $H_{\mu\nu}\ell^\mu n^\nu$ involves two terms, which are given by:

$$\begin{aligned} H'_{\mu\nu}\ell^\mu n^\nu = 2\Bigg[&4p_t\left(p_t+\frac{2}{9}\rho-\frac{4}{3}p_r\right) \\ &-\frac{2}{F^2}\{6Fp_t+(F+4\lambda)(\rho-p_r)\} \\ &-6\left\{p_t+\frac{2}{3}(\rho-p_r)-\frac{3F}{F^2}\right\}^2 \\ &+\frac{16}{9}(\rho^2+p_r^2)-72\frac{\lambda^2}{F^4}\Bigg]. \end{aligned} \tag{24}$$

The term involving the $L_{\rm GB}$ gives the following expression in terms of the matter variables:

$$\begin{aligned} L_{\rm GB} = &\left[\frac{2}{3}(\rho-p_r)-2p_t\right]^2+18\left[\frac{F^2+32\lambda^2}{F^4}\right] \\ &+6\left[p_t+\frac{2}{3}(\rho-p_r)-\frac{3F}{F^2}\right]^2-\frac{12}{9}(\rho-p_r)^2 \\ &-4\left[\frac{2}{3}(\rho+p_r)+p_t\right]^2-4\left[\frac{2}{3}(\rho+p_r)-p_t\right]^2. \end{aligned} \tag{25}$$

Using these expressions in Eq. (22), we shall understand the evolution of spherical MTTs for various collapse scenarios.

III. GRAVITATIONAL COLLAPSE FOR PRESSURELESS MATTER

Let us use the equations derived above to understand the dynamics of collapse process for pressureless matter configuration. In the absence of pressure, the EGB Eq. (11) implies that $F = F(r)$, whereas Eq. (13) gives $\alpha' = 0$. The metric function $\alpha(t,r)$ is a function of t only. This allows the rescaling of the time coordinate so that effectively $\alpha(t,r) = 0$. The metric function $\beta(t,r)$ follows from Eq. (19). This two solutions implies that the metric is given by:

$$ds^2 = -dt^2+\frac{R'^2}{1-k(r)}dr^2+R(r,t)^2d\Omega_3, \tag{26}$$

where $d\Omega_3$ is the metric of an unit round 3-sphere, and $R(t,r)$ is obtained from the Eq. (14), which gives the equation of motion of the collapsing matter configuration in 5D-EGB theory:

$$\dot{R}^2(r,t) = -k(r)-\frac{R^2}{4\lambda}+\frac{R^2}{4\lambda}\left[1+\frac{8\lambda F}{R^4}\right]^{1/2}, \tag{27}$$

where we have used Eq. (19). The function $k(r)$ can take either signatures or zero. The situation where $k(r)$ remains vanishing during the collapse process is called a marginally bound collapse, whereas the one in which $k(r)$ admits a positive signature is called a bounded collapse. We shall deal with these two cases only. The behavior for unbounded gravitational collapse in EGB theory is similar and shall not be carried out here.

Now, one has to ensure that this metric existing inside the collapsing matter cloud must be matched to an exterior static spherically symmetric metric. Such a metric is already well known as the Boulware-Deser-Wheeler solution [25,31–33]. We shall always ensure that metric of the collapsing matter cloud remains matched to an external Boulware- Deser- Wheeler solution of mass M, across a timelike hypersurface r_b. As we show in the Appendix C, such a matching leads to the condition that $F(r_b) = M$.

In the following, we shall consider a wide variety of density profiles for matter fields and note the formation of singularity and spherically symmetric trapped surfaces and horizons.

A. Marginally bound collapse

For the marginally bound collapse, we have $k = 0$. From the Eqs. (14) and (27), the equation of motion is

$$\dot{R}^2(r,t) = -\frac{R^2}{4\lambda}+\frac{R^2}{4\lambda}\left[1+\frac{8\lambda F}{R^4}\right]^{1/2}. \tag{28}$$

Using some simple substitutions and algebra we get the equation for matter shells corresponding to values of $R(r,t)$ (see also [11])

$$\begin{aligned} t_{sh} = t_s &-\left[\frac{\lambda R^2}{\sqrt{R^4-8\lambda F}-R^2}\right]^{1/2} \\ &-\frac{\sqrt{\lambda}}{2\sqrt{2}}\tan^{-1}\left[\frac{3R^2-\sqrt{R^4-8\lambda F}}{2\sqrt{2}\{\sqrt{R^4-8\lambda F}-R^2\}^{1/2}}\right], \end{aligned} \tag{29}$$

where t_s is the time of the formation of singularity, and is given by:

$$\begin{aligned} t_s = &\frac{\sqrt{\lambda}}{2\sqrt{2}}\tan^{-1}\left[\frac{3r^2-\sqrt{r^4-8\lambda F}}{2\sqrt{2}\{\sqrt{r^4-8\lambda F}-r^2\}^{1/2}}\right] \\ &+\left[\frac{\lambda r^2}{\sqrt{r^4-8\lambda F}-r^2}\right]^{1/2}. \end{aligned} \tag{30}$$

The expression of the time for shells reach the Boulware-Deser-Wheeler horizon or the MTT, obtained for $R(r,t) = \sqrt{F(r,t) - 2\lambda}$ is given by $t_{\rm MTT}$:

$$t_{\rm MTT} = t_s - \left[\frac{\lambda(F-2\lambda)}{\sqrt{(F-2\lambda)^2 - 8\lambda F} - (F-2\lambda)}\right]^{1/2} - \frac{\sqrt{\lambda}}{2\sqrt{2}}\tan^{-1}\left[\frac{3(F-2\lambda) - \sqrt{(F-2\lambda)^2 - 8\lambda F}}{2\sqrt{2}\{\sqrt{(F-2\lambda)^2 - 8\lambda F} - (F-2\lambda)\}^{1/2}}\right]. \quad (31)$$

Given these expressions we now proceeds to understand the nature of MTTs for some realistic mass profiles.

1. Examples

(1) Let us first consider a collapsing matter profile which admits a variation in the density distribution according to the choice of two parameters ς and r_0. The density distribution is of the following form:

$$\rho(r) = \frac{m_0 \mathcal{E}(\varsigma)}{r_0^4}\left[1 - \mathrm{Erf}\left\{\varsigma\left(\frac{r}{r_0} - 1\right)\right\}\right], \quad (32)$$

where $m_0 = m(r \to \infty)$ is the total mass of the cloud, r_0 is the label on the matter shell coordinate where the variation of the density with the radial coordinate is largest, i.e., $-(d\rho/dr)$ is highest. We shall choose the value of $r_0 = 2$. The parameter ς in Eq. (32) controls the variation of density function. A similar density profile was also studied for LTB models in 4-d GR [39,40]. As seen from the plot in Fig. 1(a), a larger value of ς implies a step-function-type distribution of the density, whereas, for a lower value of ς, the density varies slowly with r. So, ς is a control parameter for approach toward the OSD model—the larger the value of ς, the closer is the density to isotropy, and smaller values of ς implies inhomogeneities. The function $\mathcal{E}(\sigma)$ has the following form:

$$\mathcal{E}(\varsigma) = 3\varsigma^3[2\pi\varsigma(2\varsigma^2+3)(1+\mathrm{Erf}\varsigma) + 4\sqrt{\pi}\exp(-\varsigma)(1+\varsigma^2)]^{-1}, \quad (33)$$

and Erf is the usual error function. We consider the cases where $\varsigma = 5$ and 15. The graphs are given in Fig. 1. From Fig. 1(d), we note that as shells begin to collapse, the MTT begins to form, and grows with the fall of the shells, until the growth stops when all the shells up to $r = 2$ has fallen in. This happens since the matter density is almost zero after $r = 2$. After all the matter goes in, the MTT becomes null, as seen by the straight line in Fig. 1(d). The MTT becomes null at $R = 0.89$ since the total mass of the cloud is unity, and hence for $\lambda = 0.1$, the MTT is obtained from Eq. (21) to be $\sqrt{0.8} = 0.894$. In this region, the MTT has reached the IH phase.

Two further points need to be noticed. First, for $\varsigma = 5$, the MTT are spacelike. This may be seen from the values of C in Fig. 1(b). However, if we look at the $R(r,t) - t$ graph in Fig. 1(d), it seems that the MTT may have become timelike in certain regions. This apparent contradiction was also noted earlier in [39,48] and happens due to nontrivial ways in which the MTT crosses the chosen foliations. For $\varsigma = 15$, the MTT is surely timelike, as may be noted from Figs. 1(c) and 1(e). The MTT begins to form earlier at $r = 1.7$ at $t = 1.8$ and then begins to grow on either side to match with the MTT at the center $R = 0$, and also toward the IH at $R = 0.89$. This possibly points toward an unstable MTT, as was pointed out in the case of GR in [39,40,48].

Secondly, as can be noted from the graph in Fig. 1(e), all the shells, denoted by the blue lines reach the singularity at $R = 0$ at the same time, which is a distinctive feature of the OSD process. As the value of ς is lowered, the example of Fig. 1(d) shows that the shells begin to deviate marginally from this feature since the deviation in the density profile remains small. This also points to the fact that this collapse process is similar to that in GR, at least in this particular case of isotropic collapse.

(2) For the next example, we take the mass density to have following form [11,40]:

$$\rho(r) = m_0[1 - (r/r_0)]\Theta(100 - r) \quad (34)$$

where $\Theta(x)$ denotes the Heaviside theta function, and $r_0 = 100m_0$. The graphs of ρ, C and $R(r,t)$-t are given in the Figs. 2(a), 2(b), and 2(c) respectively. Note that the MTT begin around $t = 2900$ when the shell at $r = 50$ has already fallen in. After this growth, it remains a dynamical horizon throughout and becomes an isolated horizon only when the matter shells stops falling at $r = 100$ and all the matter has collapsed. This behavior in the $R - t$ plot is reflected in the graph of C quite faithfully.

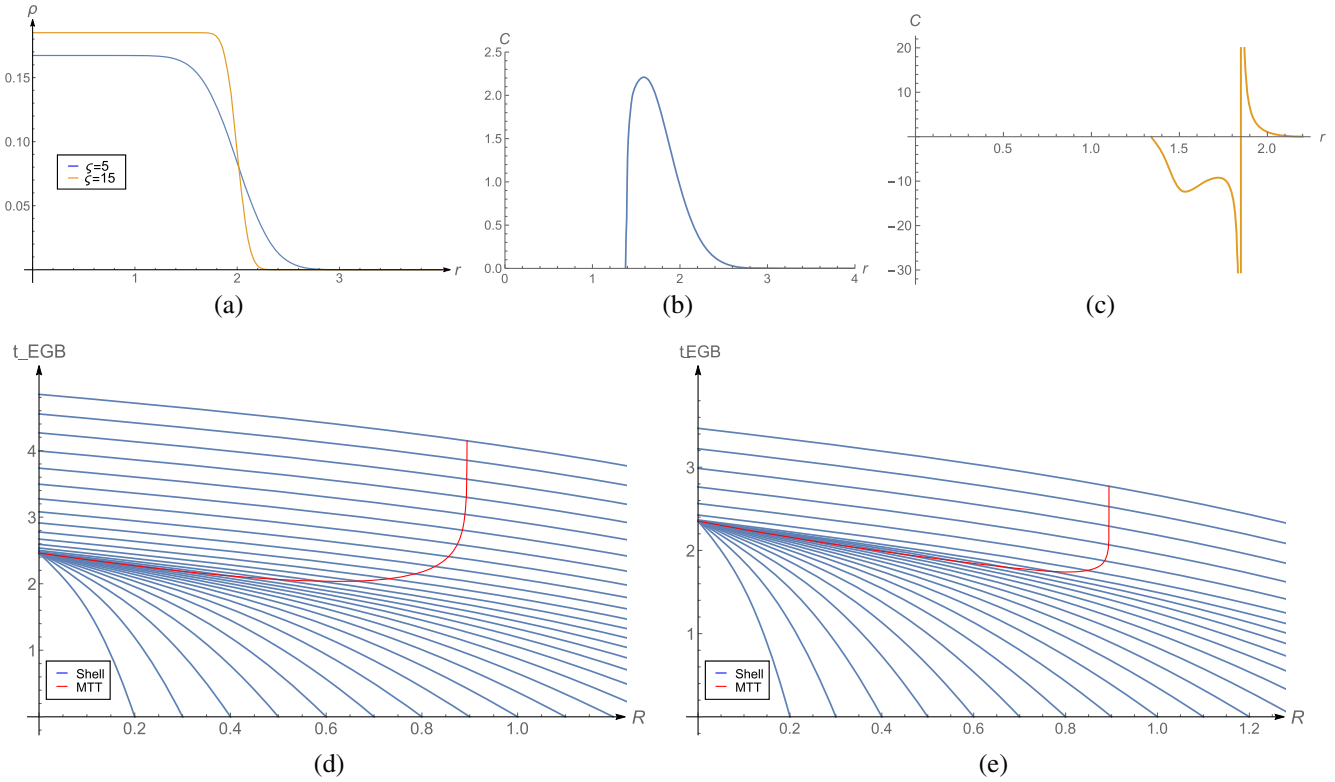

FIG. 1. These figures give the gravitational collapse for the density profile of Eq. (32). For the plot we have used the EGB coupling constant $\lambda = 0.1$. (a) gives the density fall-off for two choices of the control parameter ς, (b) is the plot of the function C for $\varsigma = 5$. The signature of C shows that the MTT in this case is spacelike. (c) is the plot of the function C for $\varsigma = 15$. The signature of C shows that the MTT in this case is timelike. The figure (d) is $R(r, t)$ vs t graph for $\varsigma = 5$, (e) gives the time development of MTT for $\varsigma = 15$ along with the collapse of each shell. In the $R - t$ graphs, the shells are denoted by blue lines whereas the red lines are the MTT. The straight vertical red lines in (d) and (e) represents the isolated horizon phase of the MTT and is reached when no more matter falls in.

Indeed, the signature of C indicates that MTT is spacelike, beginning at $r = 50$ and continues until the shell at $r = 100$ falls, after which it becomes null.

Note however that MTT does not begin to form immediately, but only after some shells have fallen in. This is because of a simple reason but leads to some important consequences, and is discussed below: The MTT forms only when the condition in Eq. (21) is satisfied. Indeed, for the early shells, the value of $F(r)$ for these shells, i.e., the amount of matter contained inside the sphere of radius r at the initial time, is smaller than the value of λ, which here is taken to be 0.1. For that reason, $R_M(r, t)$ does not admit real values. It is only after sufficient number of shells have fallen in, that condition of trapped surface can be evaluated to obtain a real value. Until that time, the central singularity remains naked for a trapped surface. Our study reveals this feature in a direct manner since we have been able to probe each and every matter shells quite elaborately.

(3) Let us now consider a Gaussian density profile with the density given by the following form:

$$\rho(r) = \frac{3m_0}{r_0^4}\exp(-r^2/r_0^2), \tag{35}$$

where m_0 is the total mass of the matter cloud, r_0 is a parameter which indicates the distance where the density of the cloud decreases to $[\rho(0)/e]$. In our example, we have chosen $r_0 = 100m_0$ and the EGB coupling constant $\lambda = 0.1$. Note that the MTT begins only after the shell at $r = 90$ has fallen in. As explained in the previous subsection, this is a direct consequence of the relation Eq. (21). The MTT in Figs. 3(b) and 3(c) clearly shows that the MTT is spacelike, and attains the IH phase when the shells at $r = 300$ has fallen in.

(4) Let us consider a density profile given by the following form for $r \in [0, \pi r_0]$:

$$\rho(r) = (\gamma/r_0^2)[\pi - (r/5r_0)\{3 + 2\cos^2(5r/r_0)\}] \tag{36}$$

where γ is a dimensionless constant. This example constitutes a situation where the MTTs are a series of timelike membranes interspaced with dynamical horizons. A similar profile was used to study gravitational collapse in 4d GR [39,40]. In our

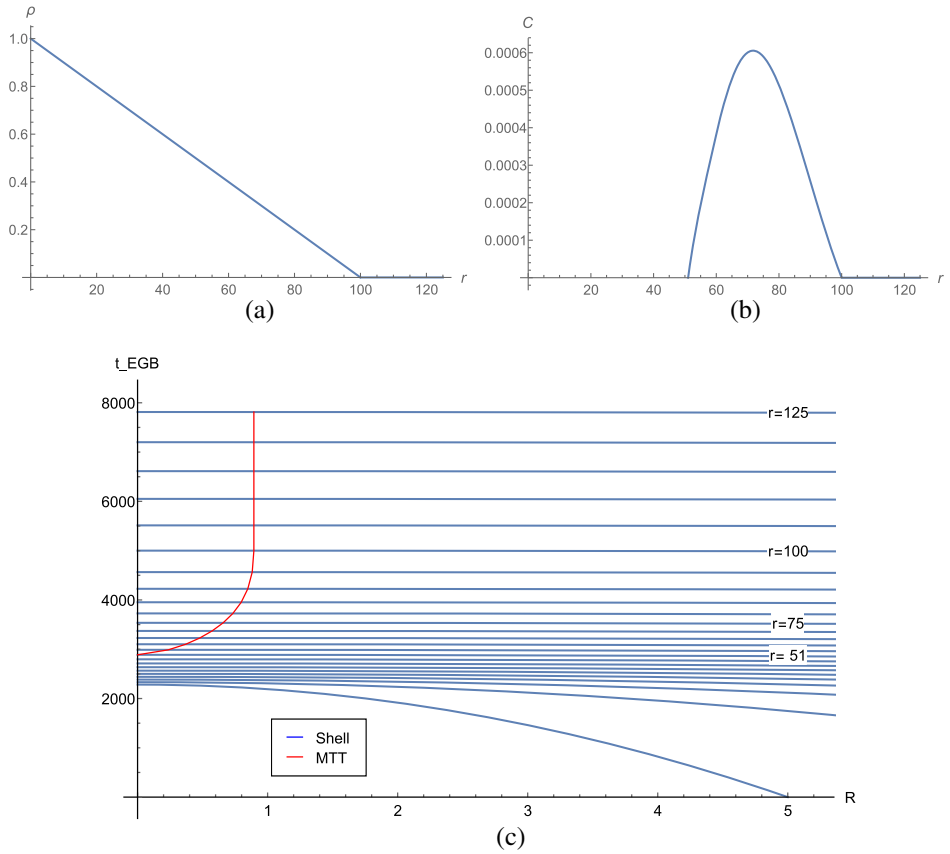

FIG. 2. The graphs show the (a) density distribution ρ, for Eq. (34), (b) values of C, and (c) formation of MTT along with the shells. For the plot we have used $\lambda = 0.1$. Note that the MTT begins to form only after some shells have fallen in the singularity. This is a direct consequence of the fact that Eq. (21) requires the mass function $F(r)$ to exceed 2λ for a real valued $R_M(r,t)$ in the equation of MTS.

example, we have chosen $r_0 = 1$, $\gamma = 1/120$, and the EGB coupling constant $\lambda = 0.1$. Note the peculiar dynamics of the MTT from Fig. 4(c). The MTT first forms for the shell at $r = 1.5$, and then evolves in a timelike manner to reach toward the MTT formed after the shells at $r = 1.35$ have fallen in. Again note that during the initial period, the central singularity is not covered by the MTT and remains naked, as expected due to Eq. (21). During the period the shells from $r = 1.7$ to $r = 2.0$ collapse, the MTT is a dynamical horizon, as may also be confirmed from the graph of C in Fig. 4(b). This behavior is repeated until matter stops falling at $r = 3.0$, when the MTT reaches the equilibrium state of an IH.

(5) Two shells falling consecutively on a black hole: Let us assume that a black hole of mass M exists, upon which a density profile of the following form falls:

$$\rho(r) = \frac{12(m_0/r_0^4)[(r/r_0) - \varsigma]^2}{[2(4+\varsigma^2) + (9+2\varsigma^2)\sqrt{\pi}e^{\varsigma^2}\{1+\varsigma \mathrm{Erf}(\varsigma)\}] \times \exp[(2r/r_0)\varsigma - (r/r_0)^2]}, \tag{37}$$

where $m_0 = M/2$, $(M = 1)$ is the mass of the shell, $2r_0$ is the width of each shell, and $\varsigma = 10m_0$. The graphs corresponding to this case is given in Eq. 5. Note that these graphs constitute the case where two mass profiles fall on a black hole one after the other. The spacetime singularity already exists into which these shells fall in. Note that as the first profile falls, the MTT begins from the already existing horizon at $R = 0.89$ and develops until the shells corresponding to $r = 23$ to $r = 25$ fall in carrying no mass with them. At these times, the MTT reaches an equilibrium state, and becomes dynamical only after the second mass profile begins to fall. So, the MTT passes through multiple stages of dynamical horizon, interspaced with isolated horizons when no matter is infalling. This behavior is easily verifiable from Figs. 5(b), and 5(c).

B. Bounded collapse

For bounded collapse, we again have $\alpha' = 0$ and $G(r,t) = e^{-2\beta(r,t)}R'^2 = 1 - k(r) = E(r)$, where $E(r)$ is the integration function. For this case $k > 0$, the equation of motion is given by (27)

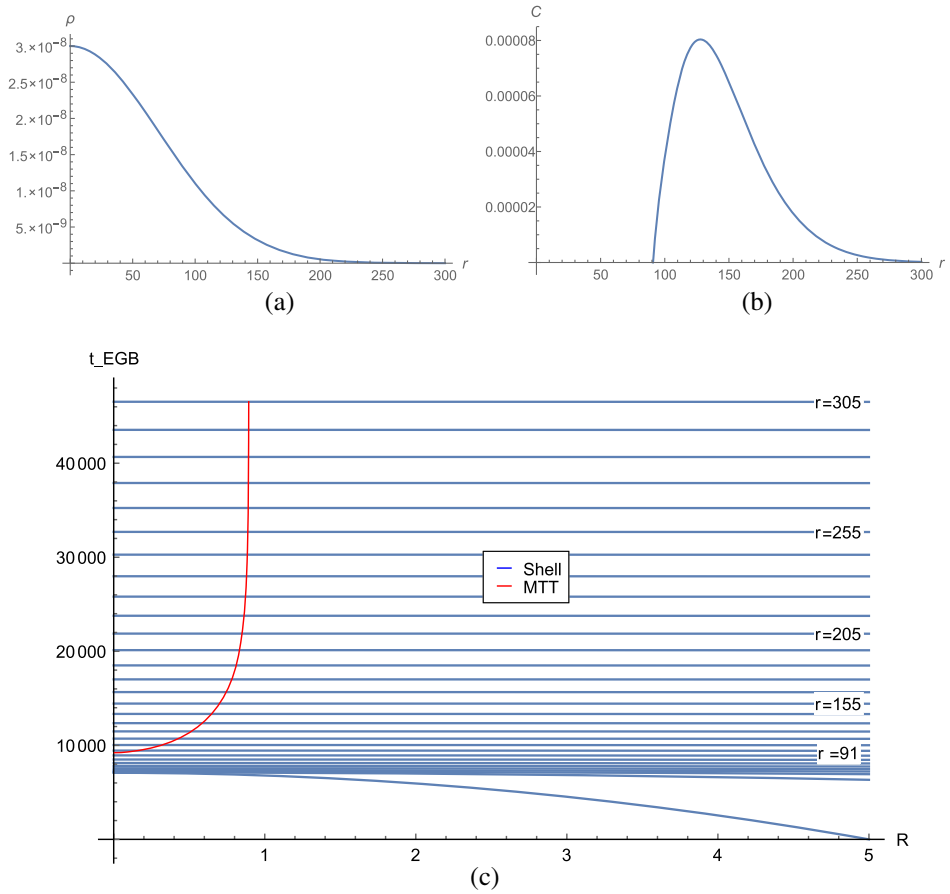

FIG. 3. The graphs show the (a) density distribution for Eq. (35), (b) values of C, and (c) formation of MTT along with the shells. The straight lines of MTT in (c), after the shell $r = 300$, represents the isolated horizon phase.

$$\dot{R}^2(r,t) = -k(r) - \frac{R^2(r,t)}{4\lambda} + \frac{R^2(r,t)}{4\lambda}\left[1 + \frac{8\lambda F(r,t)}{R^4(r,t)}\right]^{1/2}. \tag{38}$$

This equation of motion (38) can be rewritten in the following form:

$$dt = -\frac{2\sqrt{\lambda}dR}{\sqrt{-R^2 - 4\lambda k + \sqrt{R^4 + 8\lambda F}}} \tag{39}$$

To integrate this equation of motion (39), we consider a parametric choice of $R(r,t)$ of the following form:

$$x = -R^2(r,t) - 4\lambda k(r) + \sqrt{R^4(r,t) + 8\lambda F(r)}. \tag{40}$$

A simple calculation of squaring both sides leads to the following expression:

$$R(r,t) = \frac{1}{\sqrt{2}}\left[\frac{8\lambda F}{(x+4\lambda k)} - (x+4\lambda k)\right]^{1/2}. \tag{41}$$

Using this expression of Eq. (41), a simple calculation leads to modification of (39):

$$dt = \frac{\sqrt{\lambda}((x+4\lambda k)^2 + 8\lambda F)dx}{\sqrt{2}\sqrt{x}(x+4\lambda k)^{3/2}\sqrt{8\lambda F - (x+4\lambda k)^2}}. \tag{42}$$

The integration of the above equation gives the equation of the collapsing shell to be

$$\begin{aligned} t_{sh} = {} & A_1[(8\lambda F - 2\sqrt{2\lambda F}(x+4\lambda k)) + A_2\{(\sqrt{2F} + 2\sqrt{\lambda}k)\text{EllipticE}[N_1, 2N_2] \\ & - (\sqrt{2F} - 2\sqrt{\lambda}k)\text{EllipticF}[N_1, 2N_2] - 2\sqrt{\lambda}k\text{EllipticPi}[N_2, N_1, 2N_2]\}] \\ & - (A_1)_0[(8\lambda F - 2\sqrt{2\lambda F}(x_0+4\lambda k)) + (A_2)_0\{(\sqrt{2F} + 2\sqrt{\lambda}k)\text{EllipticE}[(N_1)_0, 2N_2] \\ & - (\sqrt{2F} - 2\sqrt{\lambda}k)\text{EllipticF}[(N_1)_0, 2N_2] - 2\sqrt{\lambda}k\text{EllipticPi}[N_2, (N_1)_0, 2N_2]\}]. \end{aligned} \tag{43}$$

The equation for the spherical MTTs, are obtained for $R(r,t) = \sqrt{F(r) - 2\lambda}$ and gives:

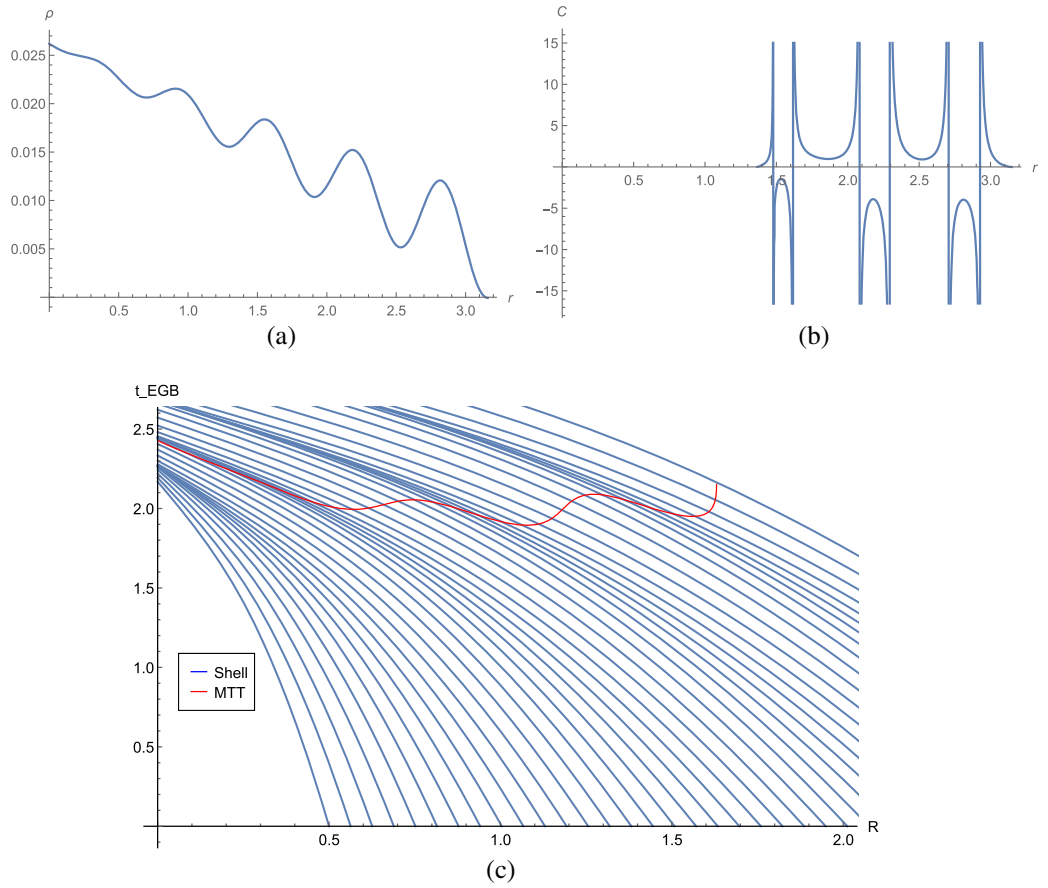

FIG. 4. The graphs show the (a) density distribution, (b) values of C, and (c) formation of MTT along with the shells for the density in Eq. (36).

$$
\begin{aligned}
t_{\mathrm{MTT}} = {} & (A_1)_{2M}[(8\lambda F - 2\sqrt{2\lambda F}(x_{2m} + 4\lambda k)) + (A_2)_{2M}\{(\sqrt{2F} + 2\sqrt{\lambda}k)\mathrm{EllipticE}[(N_1)_{2M}, 2N_2] \\
& - (\sqrt{2F} - 2\sqrt{\lambda}k)\mathrm{EllipticF}[(N_1)_{2M}, 2N_2] - 2\sqrt{\lambda}k\mathrm{EllipticPi}[N_2, (N_1)_{2M}, 2N_2]\}] \\
& - (A_1)_0[(8\lambda F - 2\sqrt{2\lambda F}(x_0 + 4\lambda k)) + (A_2)_0\{(\sqrt{2F} + 2\sqrt{\lambda}k)\mathrm{EllipticE}[(N_1)_0, 2N_2] \\
& - (\sqrt{2F} - 2\sqrt{\lambda}k)\mathrm{EllipticF}[(N_1)_0, 2N_2] - 2\sqrt{\lambda}k\mathrm{EllipticPi}[N_2, (N_1)_0, 2N_2]\}], \qquad (44)
\end{aligned}
$$

where the coefficients A_1, A_2, and the arguments N_1, N_2 are given by:

$$
\begin{aligned}
A_1 &= \frac{\sqrt{x}}{k(x + 4\lambda k)^{3/2}\sqrt{8\lambda F - (x + 4\lambda k)^2}}, \\
A_2 &= \frac{(2^5\lambda^2 F)^{1/4}\sqrt{x + 4\lambda k}\sqrt{-8\lambda F + (x + 4\lambda k)^2}}{\sqrt{x\sqrt{2F} + 2\sqrt{\lambda}k}} \\
N_1 &= \sin^{-1}\left[\frac{(\sqrt{2F} + 2\sqrt{\lambda}k)(x + 4\lambda k)}{2\lambda k\{2\sqrt{2\lambda F} + (x + 4\lambda k)\}}\right]^{1/2}, \\
N_2 &= \frac{2\sqrt{\lambda}k}{\sqrt{2F} + 2\sqrt{\lambda}k}.
\end{aligned}
$$

The t_{MTT} terms with subscript 0 and $2M$ represents its value at the initial shells at $r = r_0$ and at the formation of MTT with $R_M = \sqrt{F - 2\lambda}$. For example, $x = -R^2 - 4\lambda k + \sqrt{R^4 + 8\lambda F}$, whereas, its value at 0 represents $x_0 = -r^2 - 4\lambda k + \sqrt{r^4 + 8\lambda F}$. The EllipticF$[\phi, z]$ represents an incomplete elliptic integral of the first kind, EllipticE$[\phi, z]$ is elliptic integral of the second kind, whereas EllipticPi $[y; \phi, z]$ is an elliptic integral of the third kind [70].

In the following we shall take several examples to show how a MTT develops during the bounded gravitational collapse in EGB theory.

1. Examples

(1) Let us consider a Gaussian profile with the density given by Eq. (35). The form of the density is same as in Fig. 3(a). In our example, we have chosen $r_0 = 100m_0$. The behavior of MTT is similar to that discussed for

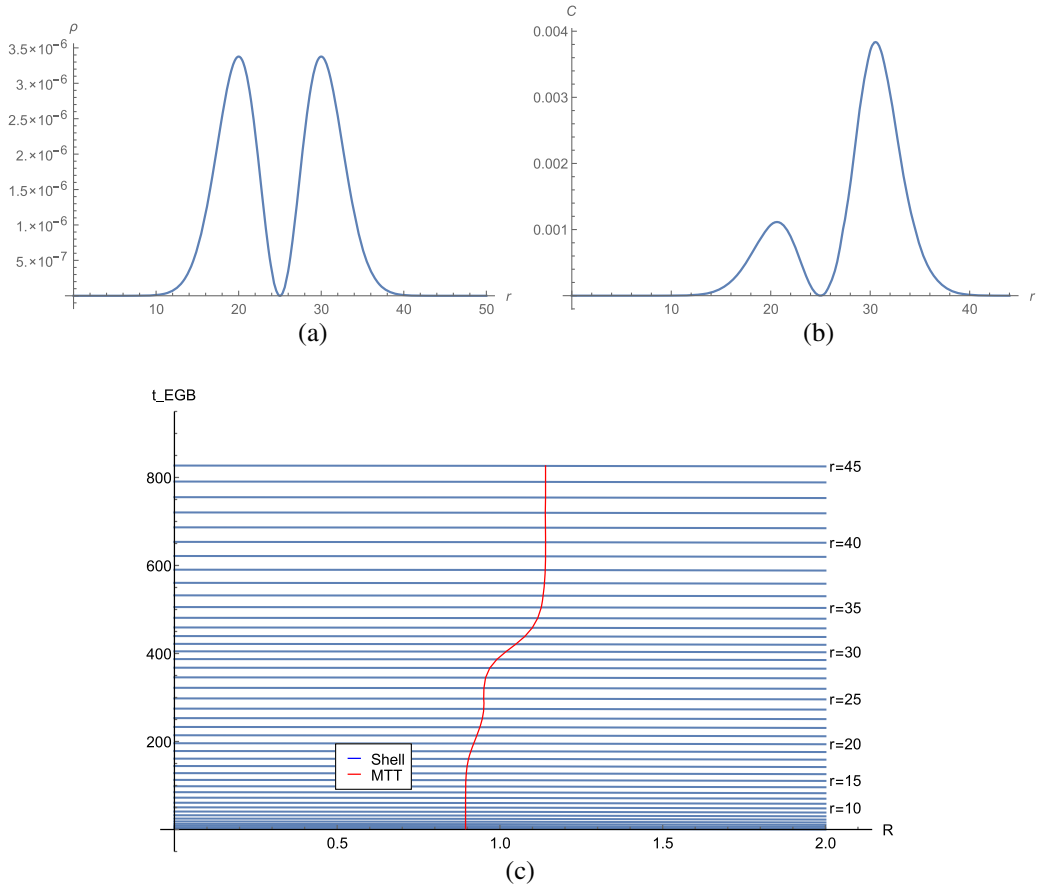

FIG. 5. The graphs show the (a) the density profile from Eq. (37), (b) values of C, and (b) formation of MTT along with the shells which fall consecutively on a black hole.

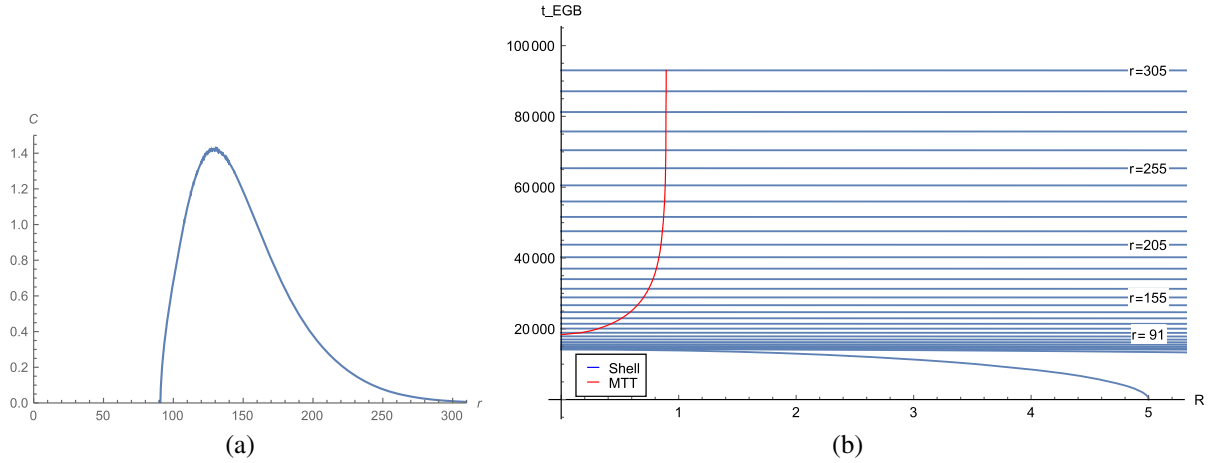

FIG. 6. The graphs show the (a) values of C, and (b) formation of MTT along with the shells for the Gaussian distribution of Eq. (35).

the marginally bound case, see Fig. 6. However, the time of formation of MTT and the value of the C has changed in comparison. Again note that the MTT forms only after shells at $r = 90$ collapse. Before that shell falls in, the singularity remains naked. The time of formation of MTT changes in comparison to the marginally bound case of Fig. 3. The straight lines of MTT in (b), after the shell $r = 300$, represents the isolated horizon phase.

(2) Let us consider a density profile given by the following form:

$$\rho(r) = (m_0/8\pi r_0^4)\exp(-r/r_0), \tag{45}$$

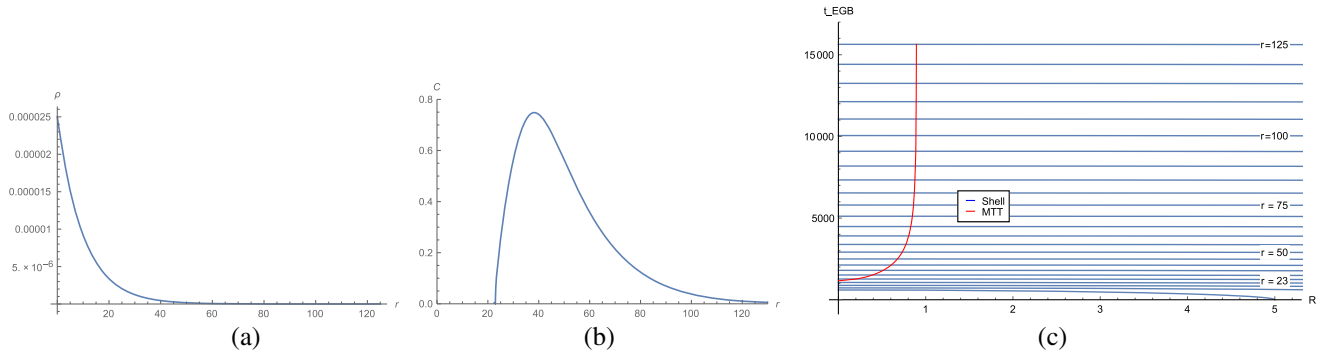

FIG. 7. The graphs show the (a) values of C, and (b) formation of MTT along with the shells for the matter profile with exponentially falling density distribution given in Eq. (45). The MTT is spacelike.

where m_0 is the total mass of the matter cloud, $r_0 = 100m_0$ is a parameter which indicates the distance where the density of the cloud decreases to $[\rho(0)/e]$. The MTT begins after the shells at $r = 30$ have fallen into the singularity. The MTT remains spacelike through out its time evolution, and reaches an equilibrium state only after the density reaches negligible values. These conclusions are easily be verified from the graphs in Fig. 7. Note again that the MTT begins only after sufficient number of shells have collapsed to the singularity in accordance to the choice of $\lambda = 0.1$ in Eq. (21).

(3) Two shells falling consecutively on a black hole: The density is given by Eq. (37). The graphs corresponding to this case is given in Fig. 8. Note that these graphs have a similar behavior to those in Fig. 5, except that the times for formation of MTTs have changed.

(4) Let us again consider the density profile given by Eq. (36), given in Fig. 4(a). The behavior is of the MTTs and the shells, for the bounded collapse as given in Fig. 9 is similar to the graphs in Fig. 4, with the exception that the time of formation of MTTs, and as well as those of the shells reaching the singularity has changed.

Similar study may be carried out for more complicated matter profiles and other matter sources. These studies can be made using the techniques developed above.

IV. GRAVITATIONAL COLLAPSE FOR FLUIDS ADMITTING TANGENTIAL PRESSURE

Let us now extend our study to matter fields which admit pressure terms in energy momentum tensor, Eq. (9). Timelike/null fluids satisfying linear equation of state are the most simple examples of this kind. They have been studied in GR to understand astrophysical black holes, but they are yet to be analysed in the EGB theory. For simplicity in obtain analytic expression, these studies have been restricted to fluids having vanishing radial pressure, but admitting dynamical tangential pressures satisfying an equation of state. These tangential pressure models of gravitational collapse have shown to lead to either a black hole or a naked singularity depending on the fluid parameters [4,71]. For comparison with GR, we shall also consider a similar model of fluids, where $p_r = 0$, and

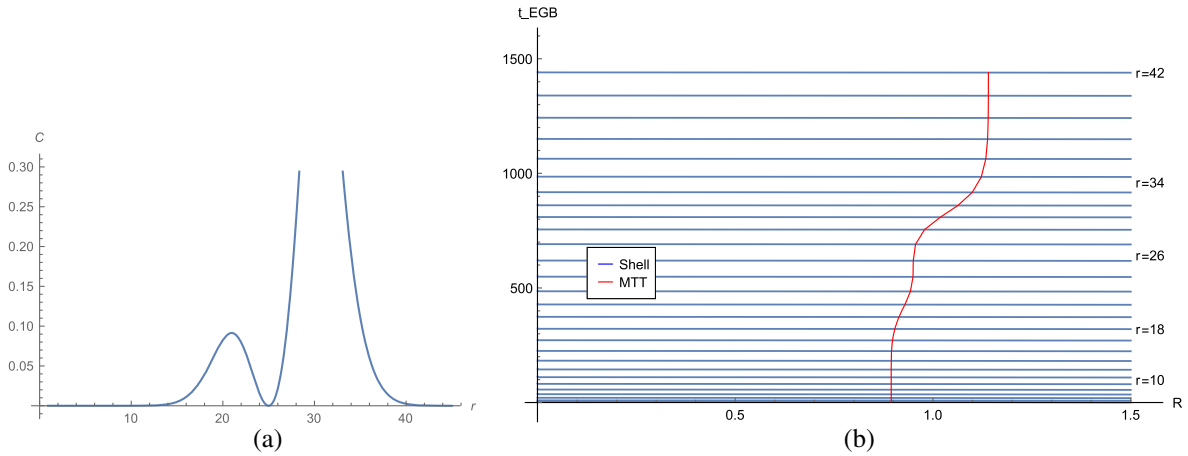

FIG. 8. The graphs show the (a) values of C, and (b) formation of MTT along with the shells which fall consecutively on a black hole. The value of C remains positive and large, and for that reason it is not plotted here. As a consequence MTT remains spacelike.

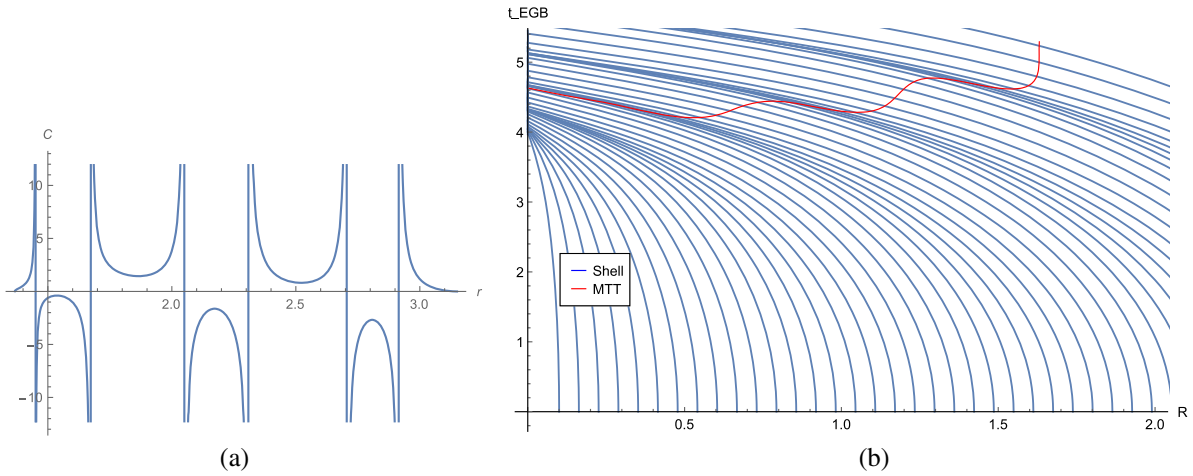

(a) (b)

FIG. 9. The graphs show the (a) density distribution, (b) values of C, and (c) formation of MTT along with the shells for the bounded collapse of the density profile discussed in Eq. (36). The MTT is quite complicated and goes through various modulations.

the tangential pressure satisfy a linear equation of state, $p_t = k\rho$, where k is the equation of state parameter.

A look at the EGB equations in Eq. (11) show that, to sustain a radial component of pressure throughout the collapse, mass function needs dependence on time as well. But since matter has no radial component of pressure, $F(r,t) = F(r)$. The Bianchi identity, Eq. (13) with the above choice gives, $\exp[\alpha(t,r)] = R^{3k}$. The Einstein equation Eq. (12) gives $\exp[\beta(t,r)] = [R'/\sqrt{b(r)}R^{3k}]$, where $b(r)$ is a integration function. Thus, the metric describing collapse of fluids admitting tangential pressure is given by:

$$ds^2 = -R^{6k}(r,t)dt^2 + \frac{R(r,t)'^2}{b(r)R^{6k}}dr^2 + R^2(t,r)d\Omega_3. \quad (46)$$

Naturally, for pressureless collapse, when $p_t = 0$, this metric reduces to Eq. (26). Again, we shall ensure that metric of the collapsing fluid remains matched to an external Boulware-Deser-Wheeler solution of mass M, across a timelike hypersurface r_b (see Appendix C). Such a matching leads to the condition that $F(r_b) = M$, and that the tangential pressure vanish on the boundary.

To study the collapse phenomena with the effects of pressure terms, we follow method used earlier. The equation for mass function Eq. (14) becomes,

$$H(r,t) = -[1 - G(r,t)] + \frac{1}{4\lambda}\left\{\sqrt{R^4 + 8\lambda F} - R^2\right\}. \quad (47)$$

Using the expressions for $G(r,t)$ and $H(r,t)$ from Eq. (46), allows us to obtain an equation for dt:

$$dt = -\frac{R^{3k}dR}{[-\{1 - b(r)R^{6k}\} + (1/4\lambda)\{\sqrt{R^4 + 8\lambda F} - R^2\}]^{1/2}} \quad (48)$$

Integration of this equation as in the previous section, leads to time equation (t_{sh}) for the shell to reach radius $R(r,t)$, the time for a shell to reach the singularity t_s, and to reach the MTT (t_{MTT}). For a distribution of matter having Gaussian distribution, and having equation of state parameter $k = 1/3$ (radiation) and for $k = 1/6$, these equations lead to the following graph in Figs. 10(a), and 10(b) These figures show that just like dust collapse, the situation for fluids is similar. The initial shells do not form trapped horizons, and the marginally trapped surface begins to form only after the collapsed matter has mass $\geq 2\lambda$.

V. DISCUSSIONS

This paper deals with the study of gravitational collapse in EGB gravity in 5-dimensions. The Gauss-Bonnet modification of the Einstein gravity changes the geometry of the spacetime, and the structure of the horizon and singularity quite drastically. We developed techniques to analyse these effects in the phenomena of gravitational collapse in this theory. In this context, several questions arise naturally regarding the process of the collapse phenomenon itself as well as the outcome of gravitational collapse of matter. To understand these details, we have, in this paper, developed a set of analytical and numerical techniques to locate spherical marginally trapped surfaces in the spacetime, when the collapse is in progress. We locate these MTTs for a large class of matter profiles and initial velocity profiles. This study helps us to address several questions regarding gravitational collapse in the EGB theory:

(i) *Role of the GB term and the coupling constant λ:* The GB term introduces several changes in the equation of motion of the gravitational field. The most drastic is the change in the form of the mass function $F(r,t)$ given in Eq. (14). In fact, this equation shows that the GB term leads to quadratic effects involving $\dot{R}(r,t)$ and $R'(r,t)$. As a result of

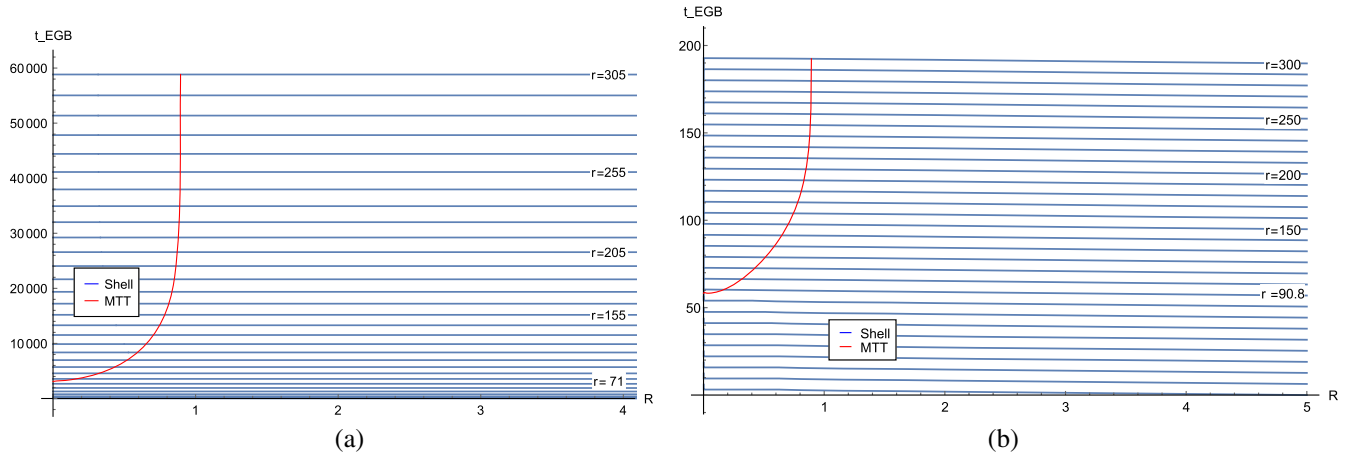

FIG. 10. The graphs show the dynamics of shell collapse for (a) $k = 1/6$, and (b) $k = 1/3$, $\lambda = 0.1$, and $b = (1/4\lambda)$, These graphs show that for fluids too, the initial shells reach the singularity a a time much earlier that trapped surfaces begin to form. The initial singularity is naked, and becomes censored only after the mass contained inside the collapsed shell $\geq 2\lambda$. The MTT forms with the $r = 70$th shell for $k = 1/6$, whereas it forms with the 90th shell for $k = 1/3$. Note also that the singularity formation time is greatly advanced for radiation fluids.

this quadratic contribution of $\dot{R}$, the equation of motion of the radius of the dust cloud is altered significantly, see Eq. (20). Naturally, this change in the equation of motion of the spherically symmetric matter configuration implies that the collapsing matter spheres will get trapped at different times. A direct reflection of this fact is in the expressions for the expansion of the outward and the inward null normals $\theta_{(\ell)}$ and $\theta_{(n)}$ in Eqs. (15) and (16). It follows as a direct result of (16) that the equation defining a marginally trapped surface is dependent on the GB coupling constant λ, see Eq. (21). The marginally trapped surface (MTS) forms at $R_M(r,t) = F(r,t)^{1/2}$ in the 5-dimensional Einstein theory, whereas it forms at $\sqrt{F(r,t) - 2\lambda}$ in the EGB theory. In this paper, we have kept the value of $\lambda = 0.1$, and so, the equation for MTS, Eq. (21) implies that real values of $R_M(r,t)$ is only possible only if sufficient number of shells have fallen in so that the cloud if massive enough to overcome the effect of the GB coupling constant λ. This effect on the formation of a MTS and the MTT is directly visible in the graphs in Fig. 2, Fig. 3 as well as in the Fig. 6. The coupling constant results in the delay in the formation of MTT, and as can be noticed from these figures, begins to form quite later than the formation of central singularity due collapsing shells. This effect is not visible in Fig. 5, since the system already has a spacetime singularity, and so, this initial black hole horizon censors all the singularities arising out of shell collapse.

It is also instructive to compare this same study of MTTs for the Gaussian profile in Eq. (35) in the 5-dimensional Einstein theory. As expected, the MTT begins just as the first shells start to collapse and the MTT equilibriates at $R = 1$, since the total mass of the profile is unity, and the MTT is $R_M(r,t) = F(r,t)^{1/2}$. This is given in Fig. 11. This difference in the behavior of dust collapse between GR and EGB, holds for tangential pressure fluid models too. Here also, in comparison with graphs in Fig. 10, the GR case has no generic nakedness of central singularities.

(ii) *Nature of the central singularity:* Since many of these configurations lead to shell collapsing *naked* singularities due to gravitational collapse of the initial shells, and that MTTs do not cover them, it becomes essential to characterize them, and make a clear classification. We have explicitly verified that, in each of the cases where the central singularity is naked initially, satisfy the following relation: *The weak cosmic censorship is violated for each of these collapse processes until the mass function* $F(r) > 2\lambda$ (see also [7]). The fact that the curvature strength of the singularity is a weak is obtained as follows: Note that the singularity is defined to be strong if the spacetime volume contained within Jacobi vector fields is reduced to zero at the singularity. The singularity is weak otherwise. According to the standard characterizations of singularities in 4-dimensions [4], a sufficient condition for a strong singularity is that at least one causal geodesic t^μ, with affine parameter v must satisfy the following condition:

$$\lim_{v \to v_0} (v - v_0)^2 R_{\mu\nu} t^\mu t^\nu > 0. \tag{49}$$

For our spacetime, and a radial timelike vector field, a simple calculation shows that $\lim_{v \to v_0} (v \to v_0)^2 R_{\mu\nu} t^\mu t^\nu = 0$. Here too, the role of

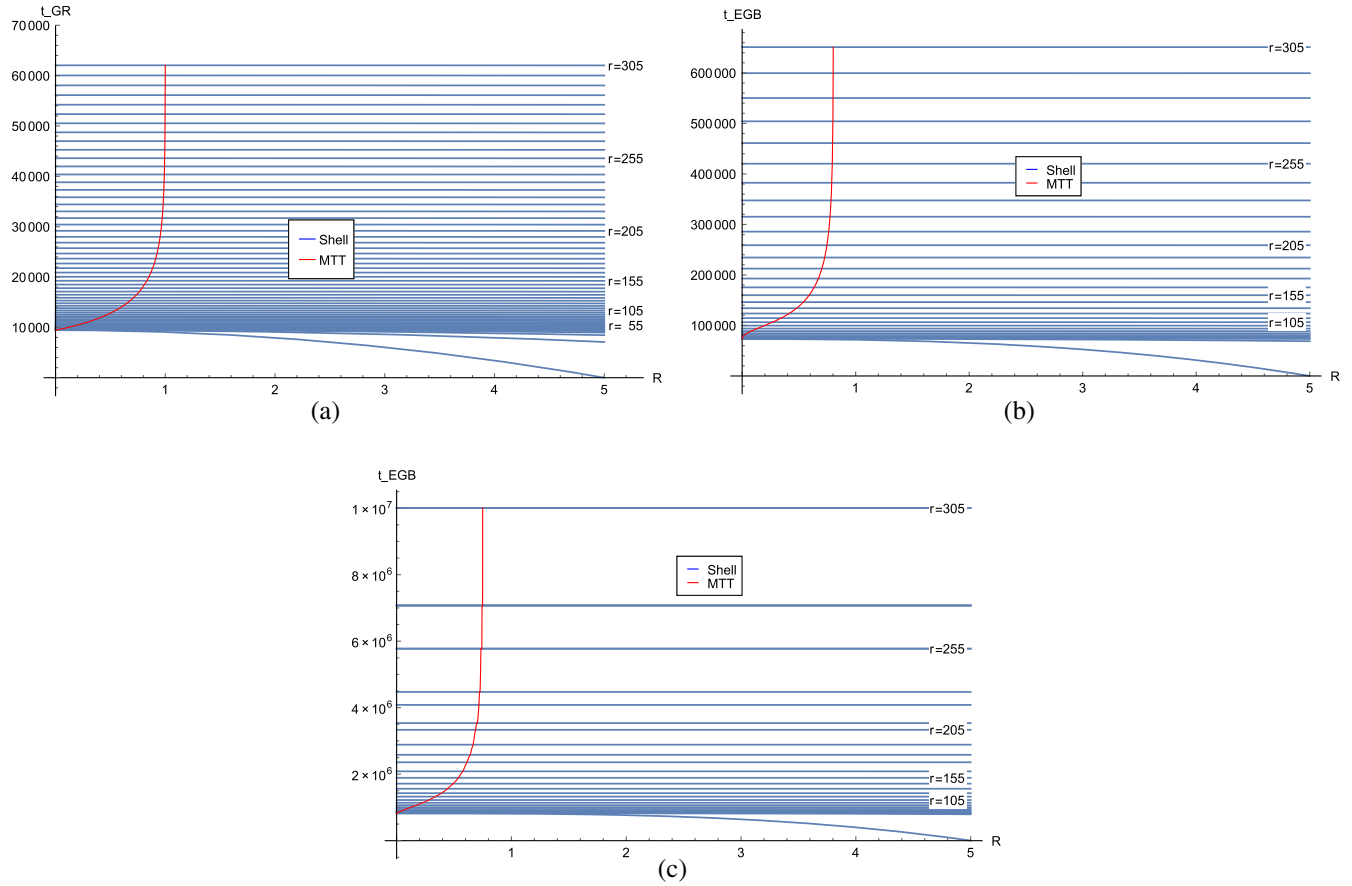

FIG. 11. The graph show formation of MTT along with the shells for marginally bound collapse of pressureless matter with a Gaussian density profile of Eq. (35), in (a) 5-dimensional GR, (b) 6-dimensional EGB and, (c) 7-dimensional EGB theory, All central singularities are censored.

the Gauss-Bonnet coupling becomes crucial, and plays an important role in weakening the singularity. So, although the singularities are naked at the beginning of the collapse process, the singularity is harmless since they are weakly naked.

(iii) *Do the results of this paper extend to higher dimensions as well?* Our main interest to look for MTTs in 5-dimensions was because of the specific form that MTT conditions $\theta_{(\ell)} = 0$, and $\theta_{(n)} < 0$ takes in that dimension. For the dust collapse studied in this paper, these conditions implied that, on the foliations of MTT, the mass function $F(r)$ must be higher than twice the GB coupling constant λ. In fact, as long as $F(r) > 2\lambda$, no MTT forms, and the singularity remains naked unless more shells collapse to the singularity and the value of $F(r)$ contained within that spherical shell is higher than 2λ. This behavior is discussed in great detail in the paper, as well as in the previous paragraphs.

For higher dimensions, MTTs do not depend on the EGB coupling λ. In fact, for dimensions higher than 5, the MTT begins with collapse of the first shell, and hence the only naked singularity for $n \geq 5$ must be massless. In the following we present the condition for formation of MTT for dimensions ≥ 5. The equation of motion for a dust shell of radius $R(r,t)$ in a n-dimensions spacetime is given by:

$$\dot{R}^2 = -k(r) - \frac{R^2}{2\lambda}\left[1 \pm \sqrt{1 + \frac{4(n-4)(n-3)\lambda F(r,t)}{R^{n-1}}}\right]. \tag{50}$$

We shall not be concerned with the positive branch since no trapped surfaces exist in that parameter space. In the negative branch, and for dust collapse (as we have been dealing with in this paper), a calculation similar to that in 5-dimensions gives the radius for the spherical marginally trapped surface for $n = 6$ to be

$$R_M = \left[(F/2) + \sqrt{(F/2)^2 + (2\lambda)^3}\right]^{1/3} \times \left[1 - \frac{2\lambda}{[F/2) + \sqrt{(F/2)^2 + (2\lambda)^3}]^{2/3}}\right] \tag{51}$$

Quite naturally, due to this form, MTT in 6 dimensions always forms along with the first matter shell

$F(r,t)=0$. For 7 dimensions, the radius of the spherical MTT is

$$R_M=[-6\lambda+\sqrt{F+36\lambda^2}]^{1/2}, \tag{52}$$

which again shows that the MTT begins at $R(r,t)=0$, when $F(r,t)=0$. One can show even more generally that, for the dust collapse in n dimensions, all massive singularities for dimensions $n\geq 6$ are censored, while all naked singularities must be massless. This implies that no future directed outgoing geodesic can emerge from the singularity [7]. In Fig. 11(b) and Fig. 11(c), we give the $R(r,t)$ graphs for the dimensions 6 and 7 respectively, as an explicit solution.

(iv) *Are MTT true black hole boundaries?* The actual extent of a black hole region is a matter of great debate. Over the years, global as well as quasilocal considerations have led to several formulations of horizon. Out of them, event horizon and Killing horizons have been quite useful in the study of black holes. The quasilocal formulations based on trapped surfaces, and in particular the definitions of trapping horizons and MTTs [47,61] have also been extensively used to prove classical and quantum laws of black hole dynamics. Although, it must also be pointed out that the formulation of MTT as a black hole boundary may need modifications, in particular in respect to the conditions on $\theta_{(n)}$, they may be quite useful for this purpose. However, the main issue lies in locating the nonspherically symmetric MTTs as well, and in the context of 4-dimensional spacetimes, they are yet to be completely specified [64–66]. Furthermore, for some spacetimes, the black hole boundary is identical with the event horizon [72,73]. Our study using spherical MTTs in 5-dimensions show that they may indeed be used as a boundary of a black hole region, although a nonspherical MTTs and their location is equally important to be understood in this context. We must also point out that our study needs to be extended for more general matter fields and geometries, so that such questions may be included in our discussions.

To conclude, we have explicitly shown, with a wide range of examples, that the nature of trapped surface, its formation and time development, is intimately related to the initial velocity and the initial density profile of the matter fields. Additionally, due to the presence of the EGB coupling constant λ, the formation of MTT gets delayed further, depending on the amount of matter a particular matter shell encloses within its boundaries. All these effects have been conclusively demonstrated through the examples considered in the main part of the paper. We must however admit that a full understanding of these phenomenon of gravitational collapse and the censorship conjecture shall require the methods of nonspherical gravitational collapse.

ACKNOWLEDGMENTS

The author A. C. is supported through the Department of Atomic Energy Project No. DAE-BRNS-58/14/25/2019, and by the Department of Science and Technology scheme of government of India through their Grant No. DST-MATRICS MTR-/2019/000916. A. G. acknowledges the support through grants from the NSF of China with Grant No. 11947301 and Fundamental Research Funds for Central universities under Grant No. WK2030000036.

APPENDIX A: EXPRESSIONS FOR CURVATURE USING MATTER VARIABLES

In the following, we collect the expressions of the various curvature components for the metric (8). These components have been used in the main part of the paper to determine the evolution of MTT, and in determining the signature of the MTT in Eq. (22). The quantities like the Ricci scalar (R_s), Ricci tensors and the Riemann tensors in terms of the energy density, radial and tangential pressure, and mass function.

First, the Riemann tensors are obtained using the metric functions and the matter variables:

$$\begin{aligned}
&R_{\theta\phi\theta\phi}=F(r,t)\sin^2\theta, \qquad R_{\theta\psi\theta\psi}=\sin^2\theta R_{\theta\phi\theta\phi}, \qquad R_{\phi\psi\phi\psi}=\sin^2\theta\sin^2\phi R_{\theta\phi\theta\phi},\\
&R_{t\phi t\phi}=\sin^2\theta R_{t\theta t\theta}, \qquad R_{t\psi t\psi}=\sin^2\theta\sin^2\phi R_{t\theta t\theta}, \qquad R_{t\theta r\theta}=0,\\
&R_{r\phi r\phi}=\sin^2\theta R_{r\theta r\theta}, \qquad R_{r\psi r\psi}=\sin^2\theta\sin^2\phi R_{r\theta r\theta},\\
&R_{t\theta t\theta}=-(1/2)e^{2\alpha}\frac{R}{\dot{R}}\frac{d}{dt}\left[\frac{F(r,t)}{R^2(r,t)}-1\right],\\
&R_{r\theta r\theta}=(1/2)e^{2\beta}\frac{R}{R'}\frac{d}{dr}\left[\frac{F(t,r)}{R^2(t,r)}-1\right],\\
&R_{rtrt}=[p_t-(2/3)(\rho+p_r)-(3F/R^4)]e^{2(\alpha+\beta)}.
\end{aligned}$$

The Ricci tensors are obtained similarly using the metric in Eq. (8).

$$R_{tt} = (-2\rho/3 + p_r/3 + p_t)e^{2\alpha}, \qquad R_{rr} = (-\rho/3 + 2p_r/3 - p_t)e^{2\beta},$$
$$R_{\theta\theta} = -(R^2/3)(\rho + p_r), \qquad R_{\phi\phi} = \sin^2\theta R_{\theta\theta},$$
$$R_{\psi\psi} = \sin^2\theta \sin^2\phi R_{\theta\theta}, \qquad R_{rt} = 0.$$

The Ricci scalar is given by $R_s = -(2/3)(\rho + p_r) - 2p_t$. Using these expressions, and the expressions for null normals in Eqs. (15) and (16), it can be shown easily that:

$$H_{\mu\nu}\ell^\mu\ell^\nu = 2\left[\frac{6F(\rho + p_r)}{F^2} + 2p_t^2 - 4p_r p_t - \frac{2}{3}p_t(\rho + p_r)\right],$$
$$H'_{\mu\nu}\ell^\mu n^\nu = 2\left[4p_t\left(p_t + \frac{2}{9}\rho - \frac{4}{3}p_r\right) - \frac{2}{F^2}\{6Fp_t + (F + 4\lambda)(\rho - p_r)\}\right.$$
$$\left. - 6\left\{p_t + \frac{2}{3}(\rho - p_r) - \frac{3F}{F^2}\right\}^2 + \frac{16}{9}(\rho^2 + p_r^2) - 72\frac{\lambda^2}{F^4}\right].$$

We can also similarly determine an expression for $L_{\rm GB}$ in terms of matter variables and the mass function.

$$L_{\rm GB} = \left[\frac{2}{3}(\rho - p_r) - 2p_t\right]^2 + 18\left[\frac{F^2 + 32\lambda^2}{F^4}\right] + 6\left[p_t + \frac{2}{3}(\rho - p_r) - \frac{3F}{F^2}\right]^2$$
$$- \frac{12}{9}(\rho - p_r)^2 - 4\left[\frac{2}{3}(\rho + p_r) + p_t\right]^2 - 4\left[\frac{2}{3}(\rho + p_r) - p_t\right]^2.$$

APPENDIX B: THREE- SURFACE GEOMETRY

The subspace in our problem is a three dimensional sphere. To understand the geometry of this subspace, we shall present a general formulation of subspaces. Let $(\mathcal{M}, g_{\mu\nu}, \nabla_\mu)$ be a 5-dimensional time- oriented spacetime with a metric compatible covariant derivative $\nabla_\mu g_{\nu\lambda} = 0$. Let us assume that $\mathcal{S}$ be a closed, orientable, spacelike 3- surface embedded in $\mathcal{M}$. Let us denote the two future pointing null vectors by ℓ^μ (outward pointing) and n^μ (inward pointing), such that $\ell \cdot n = -1$.

The induced metric h_{ab} on the 3- surface $\mathcal{S}$ is given by:

$$h_{ab} = e^\mu{}_a e^\nu{}_b g_{\mu\nu}, \tag{B1}$$

where $e^\mu{}_a$ denotes the pullback map, and $a, b, \ldots$ indicate indices on $\mathcal{S}$. The functions $e^\mu{}_a$ are orthogonal to ℓ^μ and n^μ. This implies that the pushforward of the inverse three-metric h^{ab} is given by:

$$g^{\mu\nu} = e^\mu{}_a e^\nu{}_b h^{ab} - \ell^\mu n^\nu - \ell^\nu n^\mu. \tag{B2}$$

The second quantities of importance are the extrinsic curvatures. This is vector on the normal bundle $N(\mathcal{S})$ of $\mathcal{S}$, and it has two components.

$$k^{(\ell)}{}_{ab} = e^\mu{}_a e^\nu{}_b \nabla_\mu \ell_\nu, \qquad k^{(n)}{}_{ab} = e^\mu{}_a e^\nu{}_b \nabla_\mu n_\nu, \tag{B3}$$

where the extrinsic curvature itself may be written as:

$$k^\mu{}_{ab} = k^{(n)}{}_{ab}\ell^\mu + k^{(\ell)}{}_{ab} n^\mu. \tag{B4}$$

The Riemann tensor on $\mathcal{M}$ and on $\mathcal{S}$ are given respectively by:

$$(\nabla_\mu\nabla_\nu - \nabla_\nu\nabla_\mu)Z_\lambda = R_{\mu\nu\lambda\sigma}Z^\sigma \tag{B5}$$
$$(\mathcal{D}_a\mathcal{D}_b - \mathcal{D}_b\mathcal{D}_a)z_c = \mathcal{R}_{abcd}z^d, \tag{B6}$$

where $\mathcal{D}$ is the metric compatible derivative operator on $\mathcal{S}$, so that $\mathcal{D}_a h_{bc} = 0$. The Gauss equation for the spacetime and submanifold gives the following equation:

$$e^\mu{}_a e^\nu{}_b e^\lambda{}_c e^\sigma{}_d R_{\mu\nu\lambda\sigma} = \mathcal{R}_{abcd} - \{k^{(\ell)}{}_{ac}k^{(n)}{}_{bd} + k^{(n)}{}_{ac}k^{(\ell)}{}_{bd}\}$$
$$+ \{k^{(\ell)}{}_{ad}k^{(n)}{}_{bc} + k^{(n)}{}_{ad}k^{(\ell)}{}_{bc}\}, \tag{B7}$$

and the Codazzi equations may be written in the following forms corresponding to each of the two normals:

$$e^\mu{}_a e^\nu{}_b e^\lambda{}_c \ell^\sigma R_{\mu\nu\lambda\sigma} = (D_b - \omega_b)k^{(\ell)}{}_{ac} - (D_a - \omega_a)k^{(\ell)}{}_{bc} \tag{B8}$$

$$e^\mu{}_a e^\nu{}_b e^\lambda{}_c n^\sigma R_{\mu\nu\lambda\sigma} = (D_b - \omega_b)k^{(n)}{}_{ac} - (D_a - \omega_a)k^{(n)}{}_{bc}, \tag{B9}$$

where $\omega_{\underset{\leftarrow}{a}} \equiv e^\mu{}_a\omega_\mu$ is the pullback of the connection on the normal bundle $\mathcal{N}(\mathcal{S})$, and is defined using the equation for the Shape operator to get: $\omega_{\underset{\leftarrow}{a}} = -n_\sigma e^\lambda{}_a \nabla_\lambda \ell^\sigma$.

The variation of the submanifold $\mathcal{S}$ in the normal direction $N^\mu = A\ell^\mu - Bn^\mu$ where A and B are functions on foliation, is given by the variation of the above-mentioned spacetime variables. The variation in the induced metric is:

$$\nabla_N h_{ab} = 2Ak^{(\ell)}_{ab} - 2Bk^{(n)}_{ab} \tag{B10}$$

whereas, the variation of the area element $\sqrt{h} = \sqrt{\det h_{ab}}$ is given by:

$$\nabla_N \sqrt{h} = (1/2)\sqrt{h}h^{ab}\nabla_N h_{ab} = (A\theta_{(\ell)} - B\theta_{(n)})\sqrt{h}. \tag{B11}$$

The extrinsic curvatures are written in terms of the expansion scalar and the shear tensors of the two null normals:

$$\begin{aligned} k^{(\ell)}{}_{ab} &= \frac{1}{(D-2)}\theta_{(\ell)}h_{ab} + \sigma^{(\ell)}_{(ab)}, \\ k^{(n)}{}_{ab} &= \frac{1}{(D-2)}\theta_{(n)}h_{ab} + \sigma^{(n)}_{(ab)} \end{aligned} \tag{B12}$$

where the expansion scalar and the shear tensors are defined as:

$$\theta_{(\ell)} = \nabla_\mu \ell^\mu - \kappa_{(\ell)} \tag{B13}$$

$$\sigma^{(\ell)}_{ab} = \left[e^\mu{}_a e^\nu{}_b - \frac{h_{ab}}{(D-2)}g^{\mu\nu}\right]\nabla_\mu \ell_\nu + \kappa_{(\ell)}h_{ab}, \tag{B14}$$

where $\kappa_{(\ell)} = -n_\nu \ell^\mu \nabla_\mu \ell^\nu$ is the measure of affinity of the null normal. These equations for the other null-normal n^μ is obtained by $\ell^\mu \leftrightarrow n^\mu$.

Let us now consider how the foliation is evolved along N^μ. Since ℓ_μ and n_μ are normal to $\mathcal{S}$, their pullback on $\mathcal{S}$ vanish. Thus, $e^\mu{}_{\underleftarrow{a}}\ell_\mu \equiv \ell_{\underleftarrow{a}} = 0$, and also the same is true for $n_{\underleftarrow{a}}$. This foliation is assumed to be preserved in the evolution under N^μ, so that $(\pounds_N \ell)_{\underleftarrow{a}} = 0$, and $(\pounds_N n)_{\underleftarrow{a}} = 0$ is assumed to hold true. These equations imply that:

$$N^\mu \nabla_\mu \ell_{\underleftarrow{a}} = \kappa_{(N)}\ell_{\underleftarrow{a}} - (D_{\underleftarrow{a}} - \omega_{\underleftarrow{a}})B, \tag{B15}$$

$$N^\mu \nabla_\mu n_{\underleftarrow{a}} = -\kappa_{(N)}n_{\underleftarrow{a}} + (D_{\underleftarrow{a}} + \omega_{\underleftarrow{a}})B, \tag{B16}$$

where $\kappa_{(N)} = -n_\mu N^\nu \nabla_\nu \ell^\mu$ is called the surface gravity corresponding to the vector field N^μ. A direct calculation leads to the following results on the variation of $\theta_{(\ell)}$ [51]

$$\begin{aligned} \nabla_N \theta_{(\ell)} - \kappa_N \theta_{(\ell)} = &-d^2 B + 2\omega^\mu d_\mu B - B[|\omega|^2 - d\omega \\ &- (\mathcal{R}/2) + G_{\mu\nu}\ell^\mu n^\nu - \theta_{(\ell)}\theta_{(n)}] \\ &- A[\sigma^2_{(\ell)} + G_{\mu\nu}\ell^\mu \ell^\nu + (1/2)\theta^2_{(\ell)}]. \end{aligned} \tag{B17}$$

Here, $\mathcal{R}$ is the scalar curvature of the round 3-sphere. Let us now show that for spherical symmetry with spherical foliation, the quantities A and B may be chosen to be constants. Note that with foliations of $t = r =$ constant, the 3-dimensional manifolds in Eq. (8) are round spherical. Thus, at any given point on the foliation, the tangents vector fields to the foliations $[\partial_\theta, \partial_\phi, \partial_\psi]$ are always *orthogonal* to the normals vector fields ∂_t and ∂_r. Thus, any normal vector at any point of the foliation shall then be independent of the angular coordinates. This implies that the diffeomorphisms generated by angle independent linear combination of ℓ^μ and n^μ shall map round spheres to round spheres. This leads to the conclusion that the normal combination of $A\ell^\mu + Bn^\mu$, with A and B constants, can be preserved for all times for this choice of foliation. Naturally, in spherical symmetry, we can choose the constants A, and B judiciously to extract the values of ℓ^μ and n^μ. To find the parameter C in Eq. (3), let us use the choice $A = 1$, and $B = 0$ in the Eq. (B17). For this choice, $N^\mu = \ell^\mu$. This implies that, on the MTT, where $\theta_{(\ell)} = 0$, the normal derivative of the expansion is given by:

$$\pounds_\ell \theta_{(\ell)} = -G_{\mu\nu}\ell^\mu \ell^\nu. \tag{B18}$$

The shear $\sigma_{(\ell)}$ vanishes due to spherical symmetry and remains so since the foliations are always spherically symmetric [44]. Again, on using $A = 0$, and $B = -1$ for which $N^\mu = n^\mu$, Eq. (B17) on MTT gives,

$$\pounds_n \theta_{(\ell)} = -\mathcal{R}/2 + G_{\mu\nu}\ell^\mu n^\nu. \tag{B19}$$

On spherical MTTs, the normal connection ω has contributions from the normal directions only, and the tangential directions can be chosen to vanish [44]. Note that since our spacetime and foliations, both are spherically symmetric, the choice of the ℓ^μ, and n^μ vectors are unambiguous. Hence, in the above Eq. (B17), the pull back of the normal connection ω and its divergence vanish on the spherical 3- sphere of MTT. These expressions in Eqs. (B18) and (B19), along with the field equations in Eq. (3) lead directly to the form of C in used in the paper.

APPENDIX C: MATCHING CONDITIONS AT SHELL BOUNDARY

In the following, we present the junction condition of a LTB metric, formed due to collapse of a spherically symmetric matter configuration, with the spherically symmetric metric due to a body of mass M. The interior LTB metric of the spacetime $\mathcal{M}^-$ is given by Eq. (26):

$$ds^2_- = -dt^2 + \frac{R'^2}{1-k(r)}dr^2 + R(r,t)^2 d\Omega_3, \tag{C1}$$

where $d\Omega_3$ is the metric of an unit round 3-sphere, and $R(t,r)$ is obtained from the Eq. (14). The metric of the

external spacetime $\mathcal{M}_+$ is the Boulware-Deser-Wheeler solution [25,31–33], which for 5-dimensions is given by:

$$ds_+^2 = -F(\bar{R})dT^2 + F(\bar{R})^{-1}d\bar{R}^2 + \bar{R}^2 d\Omega_3, \quad \text{(C2)}$$

where T and $\bar{R}$ are the time and radial coordinates in $\mathcal{M}_+$, and the metric function $F(\bar{R})$ is

$$F(\bar{R}) = 1 + \frac{\bar{R}^2}{4\lambda}\left[1 \mp \sqrt{1 + \frac{8\lambda M}{\bar{R}^4}}\right] \quad \text{(C3)}$$

gives the external vacuum solution for a spherical body of mass M when the $-$ve sign is chosen.

The matching is to be carried out at the timelike hypersurface Σ given by r_b. Let us denote the coordinates on this surface Σ to be $(\tau, \theta, \phi, \psi)$. From $\mathcal{M}^-$, we can write down the surface Σ as $f_-(r,t) = r - r_b = 0$, and hence, the induced metric on Σ is

$$ds_-^2 = -d\tau^2 + r_b^2 d\Omega_3. \quad \text{(C4)}$$

From the point of view of the exterior spacetime, the hypersurface may be described by $r = \bar{R}_\Sigma(\tau)$ and $t = T_\Sigma(\tau)$, with no change in the angular variables. The line element of the hypersurface is then given by

$$ds_+^2 = -[F(\bar{R}_\Sigma)\dot{T}_\Sigma^2 - F(\bar{R}_\Sigma)^{-1}\dot{\bar{R}}_\Sigma^2]d\tau^2 + \bar{R}_\Sigma(\tau)^2 d\Omega_3, \quad \text{(C5)}$$

where the dots imply derivative with respect to τ.

The induced metric in Eqs. (C4) and (C5) must have matched metric functions. This implies that:

$$F(\bar{R}_\Sigma)\dot{T}_\Sigma^2 - F(\bar{R}_\Sigma)^{-1}\dot{\bar{R}}_\Sigma^2 = 1 \quad \text{(C6)}$$

Now, let u^μ and n^μ denote the velocity of the matter variables and the normal to the Σ respectively. They must satisfy the conditions $u^\mu u_\mu = -1$, $n^\mu n_\mu = 1$, whereas, $u^\mu n_\mu = 0$. From the interior spacetime, the expressions of these vectors is easily obtained:

$$u^\mu = \delta_0^\mu \equiv (\partial_\tau)^\mu, \qquad n_\mu = \frac{R'}{\sqrt{1-k(r)}}(dr)_\mu. \quad \text{(C7)}$$

From the exterior spacetime, these vectors are also obtained similarly to give:

$$u^\mu = \dot{T}_\Sigma(\partial_\tau)^\mu + \dot{\bar{R}}_\Sigma(\partial_r)^\mu, \qquad n_\mu = -\dot{\bar{R}}_\Sigma(d\tau)_\mu + \dot{T}_\Sigma(dr)_\mu. \quad \text{(C8)}$$

The extrinsic curvatures are easily determined from these normals for the exterior as well the interior spacetimes:

$$K^-_{\tau\tau} = 0, \qquad K^-_{\theta\theta} = \bar{R}_\Sigma\sqrt{1-k(r_b)} \quad \text{(C9)}$$

$$K^+_{\tau\tau} = \dot{\bar{R}}_\Sigma^{-1}[\dot{F}(\bar{R}_\Sigma)\dot{T}_\Sigma + F(\bar{R}_\Sigma)\ddot{T}_\Sigma] \quad K^+_{\theta\theta} = \bar{R}_\Sigma F(\bar{R}_\Sigma)\dot{T}_\Sigma. \quad \text{(C10)}$$

The $K_{\theta\theta}$ equations imply the following relation:

$$\frac{dT_\Sigma}{d\tau} = \frac{\sqrt{1-k(r_b)}}{F(\bar{R}_\Sigma)}, \quad \text{(C11)}$$

whereas the Eq. (C6) gives the following equation for the function $\bar{R}_\Sigma$:

$$\frac{d\bar{R}_\Sigma}{d\tau} = [1 - k(r_b) - F(\bar{R}_\Sigma)]^{1/2}. \quad \text{(C12)}$$

This implies that the following relation hold good:

$$\left(\frac{d\bar{R}_\Sigma}{d\tau}\right)^2 = -k(r_b) + \frac{\bar{R}_\Sigma^2}{4\lambda}\left[1 \mp \sqrt{1 + \frac{8\lambda M}{\bar{R}_\Sigma^4}}\right]. \quad \text{(C13)}$$

A simple comparison with Eq. (27) implies that the condition $M = F(r_b)$ must be satisfied at the boundary.

[1] S. W. Hawking and G. F. R. Ellis, *The Large Scale Structure of Spacetime* (Cambridge University Press, Cambridge 1975).
[2] Robert M. Wald, *General Relativity* (University of Chicago Press, Chicago, 1984).
[3] L. D. Landau and E. M. Lifshitz, *The Classical Theory of Fields* (Pergamon Press, New York, 1975).
[4] P. S. Joshi, *Gravitational Collapse and Spacetime Singularities* (Cambridge University Press, Cambridge, England, 2007).
[5] R. Penrose, Phys. Rev. Lett. **14**, 57 (1965).
[6] R. Penrose, Riv. Nuovo Cimento **1**, 252 (1969) [Gen. Relativ. Gravit. **34**, 1141 (2002)].
[7] H. Maeda, Phys. Rev. D **73**, 104004 (2006).
[8] H. Maeda, Classical Quantum Gravity **23**, 2155 (2006).
[9] H. Maeda and M. Nozawa, Phys. Rev. D **77**, 064031 (2008).
[10] R. Giambo and S. Quintavalle, Classical Quantum Gravity **25**, 145003 (2008).
[11] S. Jhingan and S. G. Ghosh, Phys. Rev. D **81**, 024010 (2010).

[12] S. G. Ghosh and S. Jhingan, Phys. Rev. D **82**, 024017 (2010).
[13] T. Taves, C. D. Leonard, G. Kunstatter, and R. B. Mann, Classical Quantum Gravity **29**, 015012 (2012).
[14] G. Kunstatter, T. Taves, and H. Maeda, Classical Quantum Gravity **29**, 092001 (2012).
[15] C. Lanczos, Ann. Math. **39**, 842 (1938).
[16] C. Lanczos, J. Math. Phys. (N.Y.) **10**, 1057 (1969).
[17] D. Lovelock, J. Math. Phys. (N.Y.) **12**, 498 (1971.
[18] D. Lovelock, J. Math. Phys. (N.Y.) **13**, 874 (1972).
[19] I. L. Buchbinder, S. D. Odintsov, and I. L. Shapiro, *Effective Action in Quantum Gravity* (Taylor and Francis, New York, 1992).
[20] T. Biswas, E. Gerwick, T. Koivisto, and A. Mazumdar, Phys. Rev. Lett. **108**, 031101 (2012).
[21] F. Caravelli and L. Modesto, Phys. Lett. B **702**, 307 (2011).
[22] L. Modesto, J. W. Moffat, and P. Nicolini, Phys. Lett. B **695**, 397 (2011).
[23] S. Deser and P. van Nieuwenhuizen, Phys. Rev. D **10**, 401 (1974).
[24] B. Zwiebach, Phys. Lett. **156B**, 315 (1985).
[25] D. G. Boulware and S. Deser, Phys. Rev. Lett. **55**, 2656 (1985).
[26] G. Allemandi and M. Francaviglia, eConf C **0602061**, 02 (2006).
[27] S. Nojiri and S. D. Odintsov, Phys. Rev. D **62**, 064018 (2000).
[28] B. Zumino, Phys. Rep. **137**, 109 (1986).
[29] Y. Choquet-Bruhat, J. Math. Phys. (N.Y.) **29**, 1891 (1988).
[30] N. Deruelle and J. Madore, arXiv:gr-qc/0305004.
[31] J. T. Wheeler, Nucl. Phys. **B268**, 737 (1986).
[32] J. T. Wheeler, Nucl. Phys. **B273**, 732 (1986).
[33] T. Torii and H. Maeda, Phys. Rev. D **71**, 124002 (2005).
[34] T. Jacobson, G. Kang, and R. C. Myers, Phys. Rev. D **49**, 6587 (1994).
[35] T. Jacobson, G. Kang, and R. C. Myers, Phys. Rev. D **52**, 3518 (1995).
[36] A. Chatterjee and S. Sarkar, Phys. Rev. Lett. **108**, 091301 (2012).
[37] H Seifert, Gen. Relativ. Gravit. **10**, 1065 (1979).
[38] D. Ida and K. i. Nakao, Phys. Rev. D **66**, 064026 (2002).
[39] I. Booth, L. Brits, J. A. Gonzalez, and C. Van Den Broeck, Classical Quantum Gravity **23**, 413 (2006).
[40] A. Chatterjee, A. Ghosh, and S. Jaryal, Phys. Rev. D **102**, 064048 (2020).
[41] A. Ashtekar and B. Krishnan, Living Rev. Relativity **7**, 10 (2004).
[42] A. Ashtekar, J. Baez, A. Corichi, and K. Krasnov, Phys. Rev. Lett. **80**, 904 (1998).
[43] A. Ashtekar, C. Beetle, O. Dreyer, S. Fairhurst, B. Krishnan, J. Lewandowski, and J. Wisniewski, Phys. Rev. Lett. **85**, 3564 (2000).
[44] A. Ashtekar, S. Fairhurst, and B. Krishnan, Phys. Rev. D **62**, 104025 (2000).
[45] A. Ashtekar and B. Krishnan, Phys. Rev. Lett. **89**, 261101 (2002).
[46] A. Ashtekar and B. Krishnan, Phys. Rev. D **68**, 104030 (2003).
[47] A. Ashtekar and G. J. Galloway, Adv. Theor. Math. Phys. **9**, 1 (2005).
[48] L. Andersson, M. Mars, and W. Simon, Phys. Rev. Lett. **95**, 111102 (2005).
[49] I. Booth, Can. J. Phys. **83**, 1073 (2005).
[50] E. Schnetter, B. Krishnan, and F. Beyer, Phys. Rev. D **74**, 024028 (2006).
[51] I. Booth and S. Fairhurst, Phys. Rev. D **75**, 084019 (2007).
[52] L. Andersson, M. Mars, and W. Simon, Adv. Theor. Math. Phys. **12**, 853 (2008).
[53] A. Chatterjee and A. Ghosh, Phys. Rev. D **80**, 064036 (2009).
[54] A. Chatterjee, B. Chatterjee, and A. Ghosh, Phys. Rev. D **87**, 084051 (2013).
[55] A. Chatterjee and A. Ghosh, Phys. Rev. D **91**, 064054 (2015).
[56] A. Chatterjee and A. Ghosh, Phys. Rev. D **92**, 044003 (2015).
[57] A. Perez, Rep. Prog. Phys. **80**, 126901 (2017).
[58] A. Chatterjee and A. Ghosh, Phys. Rev. Lett. **125**, 041302 (2020).
[59] P. Hajicek, Phys. Rev. D **36**, 1065 (1987).
[60] R. M. Wald and V. Iyer, Phys. Rev. D **44**, R3719 (1991).
[61] S. A. Hayward, Phys. Rev. D **49**, 6467 (1994).
[62] A. Krasinski and C. Hellaby, Phys. Rev. D **69**, 043502 (2004).
[63] I. Booth and J. Martin, Phys. Rev. D **82**, 124046 (2010).
[64] I. Bengtsson and J. M. M. Senovilla, Phys. Rev. D **79**, 024027 (2009).
[65] I. Bengtsson and J. M. M. Senovilla, Phys. Rev. D **83**, 044012 (2011).
[66] I. Bengtsson, E. Jakobsson, and J. M. M. Senovilla, Phys. Rev. D **88**, 064012 (2013).
[67] I. Booth and D. W. Tian, Classical Quantum Gravity **30**, 145008 (2013).
[68] B. Creelman and I. Booth, Phys. Rev. D **95**, 124033 (2017).
[69] I. Booth, H. K. Kunduri, and A. O'Grady, Phys. Rev. D **96**, 024059 (2017).
[70] E. T. Whittaker and G. N. Watson, *A Course of Mathematical Analysis* (Cambridge University Press, Cambridge, England, 1975).
[71] R. Goswami and P. Joshi, Classical Quantum Gravity **19**, 5229 (2002).
[72] D. M. Eardley, Phys. Rev. D **57**, 2299 (1998).
[73] I. Ben-Dov, Phys. Rev. D **75**, 064007 (2007).